Materials and Structures (2025) 58:181
https://doi.org/10.1617/s11527-025-02688-9

RILEM TC REPORT

# Mechanical properties of 3D printed concrete: a RILEM 304-ADC interlaboratory study – compressive strength and modulus of elasticity

**Viktor Mechtcherine · Shravan Muthukrishnan · Annika Robens-Radermacher · Rob Wolfs · Jelle Versteege · Costantino Menna · Onur Ozturk · Nilufer Ozyurt · Josef Roupec · Christiane Richter · Jörg Jungwirth · Luiza Miranda · Rebecca Ammann · Jean-François Caron · Victor de Bono · Renate Monte · Iván Navarrete · Claudia Eugenin · Hélène Lombois-Burger · Bilal Baz · Maris Sinka · Alise Sapata · Ilhame Harbouz · Yamei Zhang · Zijian Jia · Jacques Kruger · Jean-Pierre Mostert · Mateja Štefančič · Lucija Hanžič · Abdelhak Kaci · Said Rahal · Manu Santhanam · Shantanu Bhattacherjee · Chalermwut Snguanyat · Arun Arunothayan · Zengfeng Zhao · Inka Mai · Inken Jette Rasehorn · David Böhler · Niklas Freund · Dirk Lowke · Tobias Neef · Markus Taubert · Daniel Auer · C. Maximilian Hechtl · Maximilian Dahlenburg · Laura Esposito · Richard Buswell · John Kolawole · Muhammad Nura Isa · Xingzi Liu · Zhendi Wang · Kolluru Subramaniam · Freek Bos**

Received: 28 November 2024 / Accepted: 12 May 2025 / Published online: 24 June 2025


**Abstract** Traditional construction techniques, such as in-situ casting and pre-cast concrete methods, have well-established testing protocols for assessing compressive strength and modulus of elasticity, including specific procedures for sample preparation and curing. In contrast, 3D concrete printing currently lacks standardized testing protocols, potentially contributing to the inconsistent results reported in previous studies.

This paper has been prepared by representatives of participating laboratories and a writing group within the framework of RILEM TC 304-ADC 'Assessment of Additively Manufactured Concrete Materials and Structures' and further reviewed and approved by all members of the RILEM TC 304-ADC.
**TC Chair** Viktor Mechtcherine **TC Deputy chair** Freek Bos **TC Members** Rebecca Ammann, Arun Arunothayan, Daniel Auer, Bilal Baz, Shantanu Bhattacherjee, David Böhler, Richard Buswell, Laura Caneda Martinez, Jean-François Caron, Yu Chen, Maximilian Dahlenburg, Victor de Bono, Geert De Schutter, Laura Esposito, Claudia Eugenin, Liberato Ferrara, Niklas Freund, Lukas Gebhard, Lucija Hanžič, Ilhame Harbouz, C. Maximilian Hechtl, Muhammad Nura Isa, Egor Ivaniuk, Smrati Jain, Zijian Jia, Zhengwu Jiang, Jörg Jungwirth, Abdelhak Kaci, Emmanuel Keita, John Kolawole, Jacques Kruger, Cezary Kujath, Lucas Lima, Xingzi Liu, Hélène Lombois-Burger, Dirk Lowke, Inka Mai, Costantino Menna, Luiza Miranda, Renate Monte, Sandro Moro, Jean-Pierre Mostert, Shravan Muthukrishnan, Iván Navarrete, Tobias Neef, Behzad Nematollahi, Onur Ozturk, Nilufer Ozyurt, Said Rahal, Inken Jette Rasehorn, Atta Ur Rehman, Christiane Richter, Annika Robens-Radermacher, Josef Roupec, Nicolas Roussel, Aljoša Šajna, Manu Santhanam, Alise Sapata, Maris Sinka, Chalermwut Snguanyat, Mateja Štefančič, Katarina Šter, Kolluru Subramaniam, Markus Taubert, Jörg F. Unger, Jolien Van Der Putten, Kim Van Tittelboom, Gideon van Zijl, Jelle Versteege, Zhendi Wang, Timothy Wangler, Daniel Weger, Rob Wolfs, Yamei Zhang, Yi Zhang, Zengfeng Zhao.

V. Mechtcherine · S. Muthukrishnan · T. Neef · M. Taubert
TU Dresden, Dresden, Germany

S. Muthukrishnan · A. Arunothayan
Swinburne University of Technology, Melbourne, Australia

A. Robens-Radermacher
Bundesanstalt Für Materialforschung Und -Prüfung, Berlin, Germany

To address this issue, RILEM TC 304-ADC initiated a comprehensive interlaboratory study on the mechanical properties of 3D printed concrete. This study involves 30 laboratories worldwide, contributing 34 sets of data, with some laboratories testing more than one mix design. The compressive strength and modulus of elasticity were determined under three distinct conditions: Default, where each laboratory printed according to their standard procedure followed by water bath curing; Deviation 1, which involved creating a cold joint by increasing the time interval between printing layers; and Deviation 2, where the standard printing process was used, but the specimens were cured under conditions different from water bath. Some tests were conducted at two different scales based on specimen size—"mortar-scale" and "concrete-scale"—to investigate the size effect on compressive strength. Since the mix design remained identical for both scales, the only variable was the specimen size. This paper reports on the findings from the interlaboratory study, followed by a detailed investigation into the influencing parameters such as extraction location, cold joints, number of interlayers, and curing conditions on the mechanical properties of the printed concrete. As this study includes results from laboratories worldwide, its contribution to the development of relevant standardized testing protocols is critical.

**Keywords** Additive manufacturing · Digital fabrication · Hardened concrete · Compressive strength · Young's modulus

## 1 Introduction

3D concrete printing (3DCP) is an emerging construction technology that has potential to revolutionize the construction industry through automated deposition of concrete without the need for traditional formwork. 3DCP differs from traditional construction in three major ways: (1) presence of interlayers: 3D-printed structures exhibit due to the layer-wise deposition of concrete a considerably higher number of interlayers than any traditional construction technique, leading to more pronounced anisotropy and heterogeneity; (2) exposure of concrete in plastic state: Unlike traditional methods,

R. Wolfs · J. Versteege
Eindhoven University of Technology, Eindhoven, The Netherlands

C. Menna
University of Naples Federico II, Naples, Italy

O. Ozturk · N. Ozyurt
Bogazici University, Istanbul, Turkey

J. Roupec
Brno University of Technology, Brno, Czech Republic

C. Richter · J. Jungwirth
Munich University of Applied Sciences, Munich, Germany

L. Miranda
Ghent University, Ghent, Belgium

R. Ammann
ETH Zurich, Zurich, Switzerland

J.-F. Caron · V. de Bono
Ecole Des Ponts ParisTech, Paris, France

R. Monte
University of São Paulo, São Paulo, Brazil

I. Navarrete · C. Eugenin
Pontificia Universidad Catolica de Chile, Santiago, Chile

H. Lombois-Burger · B. Baz
Holcim Innovation Center, Lyon, France

M. Sinka · A. Sapata
Riga Technical University, Riga, Latvia

I. Harbouz
Université de Sherbrooke, Sherbrooke, Canada

Y. Zhang · Z. Jia
Southeast University, Nanjing, China

J. Kruger · J.-P. Mostert
Stellenbosch University, Stellenbosch, South Africa

M. Štefančič · L. Hanžič
ZAG - Slovenian National Building and Civil Engineering Institute, Ljubljana, Slovenia

A. Kaci · S. Rahal
CY Cergy Paris Université, Cergy-Pontoise, France

M. Santhanam
Indian Institute of Technology Madras, Chennai, India

S. Bhattacherjee
Tvasta, Bengaluru, India

C. Snguanyat
SCG Cement-Building Materials, Bangkok, Thailand

where concrete is protected by formwork until it sets, 3D printed concrete is exposed to the ambient right after it exits the nozzle; and (3) higher content of fines. While a recent trend of incorporating large aggregates into printable mixes can be observed, such as the CONPrint3D approach at TU Dresden, the majority of printable mixtures are still fine-grained compositions [1, 2]. Due to these differences, the standardized testing procedures for concrete used in in-situ casting or pre-casting cannot be directly applied to 3DCP without further adjustments. Considering that, previous studies have developed modified testing procedures for 3D-printed specimens, specifically conducting compressive strength tests in three loading directions: parallel (U), lateral (V), and perpendicular (W) to the print direction, instead of single direction typically used for cast specimens [3–5]. The study by Muthukrishnan et al. [3] reported that the compressive strength in the U loading direction was the highest, followed by V and then W directions. Meanwhile, when testing compressive strength in three loading directions, Le et al. [4] found that the compressive strength was similar in U and W loading directions but was the lowest in V loading directions. In another study by Wolfs et al. [5] the compressive strength in U and V loading direction was 29.2 MPa, whereas in W loading direction it was 28.5 MPa, indicating no directional dependency. The reasons behind these discrepancies in trends remain unclear, and it is difficult to identify a specific cause due to the lack of standardization, particularly in the specimen preparation procedures. Each study employed its own methods, influenced by the capabilities of the printing equipment and the experience of the authors.

To address this issue, RILEM TC 304-ADC organized a comprehensive interlaboratory study on the mechanical properties of 3D-printed concrete. A detailed study plan was distributed to all participants to ensure consistency in sample preparation, testing methods, and documentation [6]. Special attention was given to the anisotropic behavior of printed concrete, a characteristic not typically considered in conventional cast concrete. While specific guidelines were established for sample preparation and testing, laboratories had flexibility in selecting mix designs and printing parameters in order to obtain insights that are valid across the range of printing materials and facilities currently in use. Nevertheless, to ensure consistency, certain constraints were imposed. The binder was required to be Portland cement-based. Therefore, alternative binder types such as geopolymers or gypsum were not studied. Additionally, structural fibers or any other reinforcement that could significantly enhance mechanical properties were not permitted. Meanwhile, the laboratories were given freedom to choose between a screw-type or a pump-based extrusion systems, methods of concrete transportation (e.g., pump or manual feeding to the extruder), mixing technologies (batch or continuous), etc. As a result, extensive data covering a wide range of mix designs and printing parameters were produced. Some laboratories also explored promising multicomponent mixes for printing. In multicomponent mixes, the concrete is typically delivered to nozzle in two or more streams: one for the base mix and another for buildability-enhancing additives. The base mix is formulated to be pumpable with extended open time, while additives such as viscosity modifiers, accelerators, and rapid-setting cement slurries are used to speed-up the structural build-up [7]. This approach allows achieving the rheological properties required for 3D printing without compromising pumpability or buildability. Three laboratories in this

Z. Zhao
Tongji University, Shanghai, China

I. Mai · I. J. Rasehorn
Technical University of Berlin, Berlin, Germany

D. Böhler · N. Freund · D. Lowke
Technical University of Braunschweig, Brunswick, Germany

D. Auer · C. M. Hechtl · M. Dahlenburg · F. Bos (✉)
Technical University of Munich, Munich, Germany
e-mail: freek.bos@tum.de

L. Esposito
Heidelberg Materials, Heidelberg, Germany

R. Buswell · J. Kolawole · M. N. Isa · X. Liu
Loughborough University, Loughborough, UK

Z. Wang
China Building Materials Academy, Beijing, China

K. Subramaniam
Indian Institute of Technology Hyderabad, Hyderabad, India

Interlaboratory Study (ILS) utilized multicomponent mixes to print concrete, allowing for a comparison of mechanical properties under compression with single-component mixes. In total, the study involved 30 laboratories worldwide, who contributed 34 sets of data, with some laboratories testing multiple mix designs. While the study investigated mechanical properties in both compression and tension, this paper specifically focuses on properties under compression, such as compressive strength and modulus of elasticity. The mechanical properties under tension are discussed in detail in [8], whereas a general overview of the testing program and results is presented in [9]. The nearly 5,000 individual specimen results have been collected in an SQL database that is published in [10] and discussed in [11].

This study aims to explore the variation in compressive strength and modulus of elasticity data determined by different laboratories with their specific mix designs and printing parameters. Following this, the data is analyzed to investigate the influence of various key parameters and practices relevant to characterizing the mechanical properties of the printed elements. They are:

1. Extraction location: Ideally, compressive strength should be consistent across all extraction locations. However, variations can occur due to factors such as a dry print bed, printing issues, and inconsistencies in concrete batches during the printing process. This study aims to examine the occurrence of these variations to determine whether the extraction location is a significant parameter to be considered while determining the mechanical properties under compression.
2. Print vs. cast: We investigate to which extent cast specimens represent the mechanical properties of printed elements. Additionally, we explore the influence of 3DCP as a construction technology on the mechanical properties under compression.
3. Scale factor (or size effect): In traditional cast specimens, the influence of specimen dimensions on mechanical properties under compression is fairly well documented. In 3D-printed specimens, increasing the specimen size introduces more interlayers, which can further affect the relationship between the specimen size and mechanical properties. This study provides essential insights into this relationship.
4. Cold joints and curing conditions: In large-scale printing, intermediate stoppages are likely to occur. They may lead to the formation of cold joints that can impact the overall integrity of the printed element. Moreover, industry and academia lack standardized curing conditions for 3D-printed elements. Therefore, this investigation explores the effects of cold joints and alternative curing methods (beyond the standard water-bath curing) on the mechanical properties under compression.
5. Modulus of elasticity vs compressive strength: The modulus of elasticity of printed concrete has been less frequently reported compared to compressive strength. Therefore, this study investigates the influence of interlayers on the modulus of elasticity by comparing the printed specimen results with those obtained for conventionally cast specimens. Additionally, the impact of 3DCP technology on the relationship between modulus of elasticity and compressive strength is analyzed.

With a detailed investigation on the influence of these key parameters and practices on the mechanical properties under compression, this article aims to provide comprehensive insights not just for the academic readers but also for the practitioners. These insights will serve as a foundation to create standardized testing procedures which can be eventually leveraged for the development of building codes.

## 2 Materials and methods

### 2.1 Mix design and specimen preparation

All laboratories participated in the interlaboratory study used cementitious binders to develop printable concrete for determining compressive strength and modulus of elasticity. All but three laboratories followed 1 K approach, i.e., no addition of any constituents occurred after mixing. In contrast, three laboratories used multicomponent mixes with buildability-enhancing additives such as aluminium sulphate (accelerator) and thickeners. These three laboratories utilized dynamic print head mixers to blend the components before extrusion.

Most laboratories used sand as aggregates, with a maximum particle size of approximately 2 mm, while some participants used maximum aggregate sizes up to 4 or 8 mm, and only one laboratory used gravel with a maximum particle size of 16 mm. More details on the mix design can be found in [9, 10]. The laboratories printed walls from which specimens of two different scales were extracted: "mortar-scale" and "concrete-scale". "Mortar-scale" and "concrete-scale" stands for geometries as defined in [6]. In terms of shapes, cubes and cylinders were tested for compressive strength, and prisms and cylinders were tested for modulus of elasticity [12]. The specimens were prepared under three distinct conditions: (1) Default: Each lab printed according to their standard procedure, followed by water bath curing for $28 \pm 3$ days; (2) Deviation 1: It involved creating a cold joint by increasing the time interval between printing layers and (3) Deviation 2: Standard printing process was used, but the specimens were cured under conditions different from a water bath. More details on the specimen preparation techniques can be found in [6, 9]. Specimens that significantly deviated from the defined procedure were omitted from the analysis. The threshold values for these deviations are specified in each section accordingly.

### 2.2 Experimental program

Two types of tests were performed. The first type, compressive strength tests, involved specimens that were either sawn or core-drilled from printed elements. Unlike some codes, such as [13] for mortar, the specimens for the compression test were not obtained from the remaining halves of broken flexural specimens. Three sets of specimens were extracted from different locations of the printed element (bottom, middle, and top) to evaluate the uniformity of compressive mechanical properties across various wall locations. To analyze the anisotropy, uniaxial compressive tests were performed in three directions: U, V, and W, which correspond to longitudinal, lateral, and perpendicular to printing directions, respectively. The second test type served for determining the modulus of elasticity, aiming to measure the stabilized secant modulus of elasticity in compression on prismatic and cylinder-shaped specimens. The tests were conducted according to [12]. More details on the preparation of the specimens and the testing procedures can be found in [6]. With the compressive strength and modulus of elasticity data obtained from these tests, various analyses were conducted as shown in Table 1. This table also indicates the participation of different laboratories for each type of investigation.

## 3 Test results

The laboratories participated in this study used their own printable mix designs and printing parameters, leading to considerable variations in compressive strength and modulus of elasticity data submitted for the overarching analysis. This section provides an overview of the test results and also discusses, to some extent, the variability in data provided by each laboratory. This includes the determination and handling of outliers for further analysis. The box and whisker plots shown in Figs. 1, 2, 3, 4, 5, 6 and 7 represent absolute values of compressive strength, while Fig. 8 shows absolute values of modulus of elasticity. The box-and-whisker plot provides initial visualization of average values and variation within each series. A 'series' refers to data from a specific laboratory-material combination. Data points exceeding twice the standard deviation of their series are excluded from further analysis and marked as red dots in the plot. The horizontal continuous and dashed lines represent the average values and twice their standard deviations, respectively, for all series. To the right of the box-and-whisker plot, a bar chart displays the distribution of average values across all series, with a black line indicating the normal distribution for reference. Below the box-and-whisker plot, a bar chart shows the number of specimens (n) from each series, including details on those excluded based on the two standard deviation threshold. The coefficient of variation (CV) for each series is displayed as a percentage, followed by details regarding the printing material and system information. More details on the formatting of the figure can be found in [8].

**Table 1** Analysis performed in this article and the respective laboratory participation

| Laboratory | Focus of the analysis | | | | | | | |
|---|---|---|---|---|---|---|---|---|
| | Compressive strength | Modulus of Elasticity | 3DCP vs casting on compressive strength | Effect of cold joint on compressive strength | Effect of specimen scale on compressive strength | Effect of curing condition on compressive strength | Effect of extraction location on compressive strength | Relationship between modulus of elasticity and compressive strength |
| Lab 01 | ✓ | ✓ | ✓ | | ✓ | | ✓ | ✓ |
| Lab 02 | ✓ | ✓ | ✓ | | | | ✓ | ✓ |
| Lab 03 | ✓ | ✓ | ✓ | | | | ✓ | ✓ |
| Lab 04 | ✓ | ✓ | ✓ | | | | ✓ | ✓ |
| Lab 05 | ✓ | | ✓ | | | ✓ | ✓ | |
| Lab 06 | ✓ | | ✓ | | | ✓ | ✓ | |
| Lab 07 | ✓ | ✓ | ✓ | | | ✓ | ✓ | ✓ |
| Lab 08 | ✓ | ✓ | ✓ | | | | ✓ | ✓ |
| Lab 09 | ✓ | | ✓ | | | ✓ | ✓ | |
| Lab 10 | ✓ | | ✓ | | | | | |
| Lab 11 | ✓ | | ✓ | | | | ✓ | |
| Lab 12 | ✓ | | ✓ | ✓ | | | ✓ | |
| Lab 13 | ✓ | | ✓ | ✓ | ✓ | ✓ | ✓ | |
| Lab 14 | ✓ | | ✓ | | | | ✓ | |
| Lab 15 | ✓ | ✓ | ✓ | | | | ✓ | ✓ |
| Lab 16 | ✓ | ✓ | ✓ | | | | ✓ | ✓ |
| Lab 17 | ✓ | | ✓ | | | | | |
| Lab 18 | ✓ | ✓ | ✓ | | ✓ | | ✓ | ✓ |
| Lab 19 | ✓ | ✓ | ✓ | | | ✓ | ✓ | ✓ |
| Lab 20 | ✓ | | ✓ | ✓ | | | | |
| Lab 21 | ✓ | | ✓ | | | | | |
| Lab 22 | ✓ | | ✓ | | | ✓ | | |
| Lab 23 | ✓ | ✓ | ✓ | | | ✓ | ✓ | ✓ |
| Lab 24 | ✓ | ✓ | ✓ | | | | ✓ | ✓ |
| Lab 25 | ✓ | ✓ | ✓ | | ✓ | ✓ | ✓ | ✓ |
| Lab 26 | ✓ | | ✓ | | | | ✓ | |
| Lab 27 | ✓ | | ✓ | | | ✓ | ✓ | |
| Lab 28 | ✓ | ✓ | ✓ | | | | ✓ | ✓ |
| Lab 29 | ✓ | | ✓ | | | | ✓ | |
| Lab 30 | ✓ | | ✓ | ✓ | ✓ | | ✓ | |

### 3.1 Observations on compressive strength of printed specimens

Figures 1, 2, 3 and 4 represent absolute values of compressive strength as provided by the participating labs. In most cases, the reasons behind pronounced scatterings in the compressive strength data, also resulting in outliers, was not explicitly identified. However, in some laboratories, premature specimen failure, likely caused by eccentric loading, was observed, as shown in Fig. 5a. Unlike cast specimens, printed specimens must be precisely extracted and ground to ensure parallel surfaces and avoid eccentricity during loading. However, achieving a parallel surface through grinding is challenging. Some laboratories investigated an alternative approach by adding a thin leveling layer, commonly referred to as capping. While this method significantly reduces the effort required for grinding, this could still result in outliers on an otherwise small scatter, as, in the case


**Fig. 1** Compressive strength data reported by laboratories for mortar-scale printed specimens in (a) U loading direction (b) V loading direction and (c) W loading direction. These specimens were prepared in Default conditions

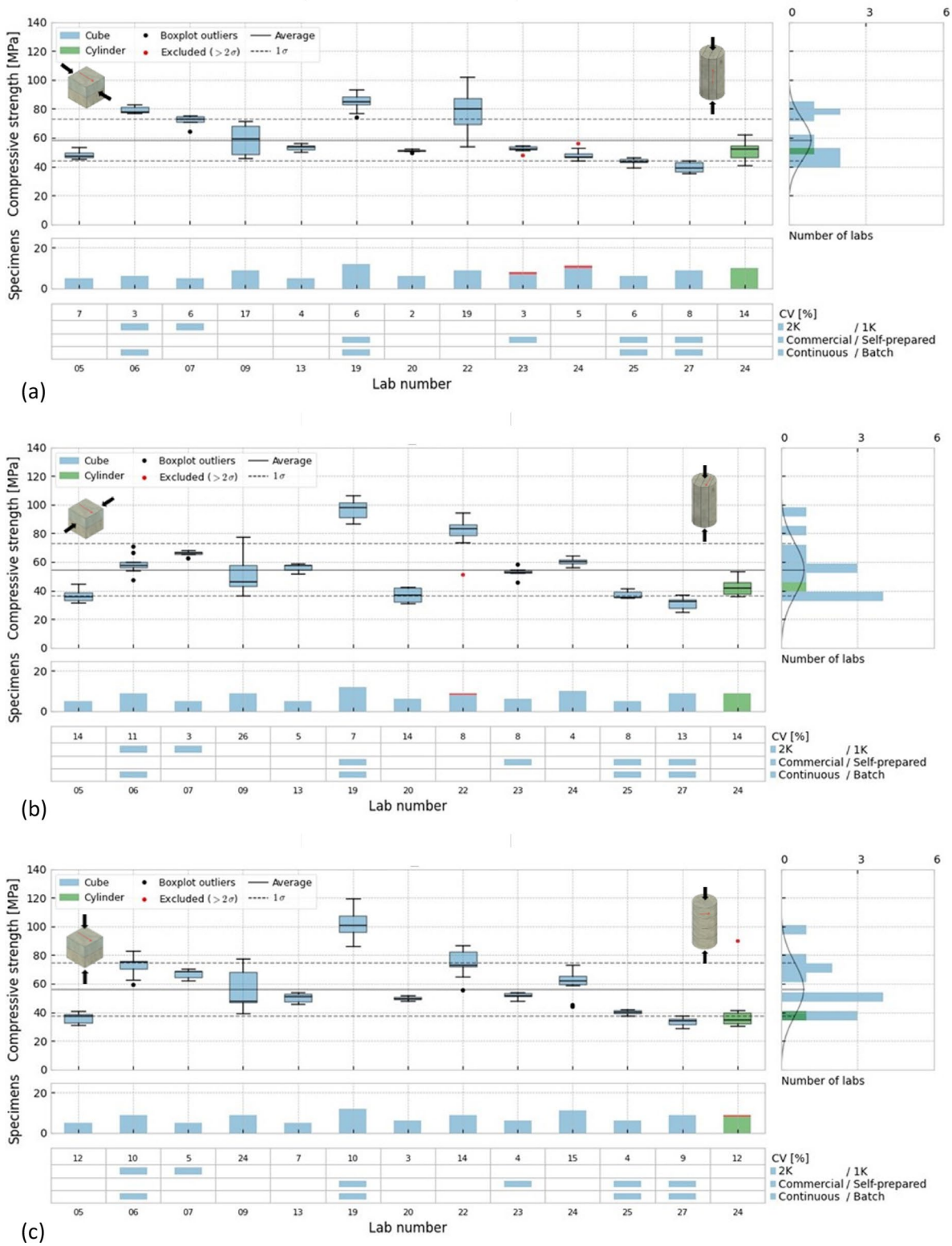


**Fig. 2** Compressive strength data reported by laboratories for mortar-scale printed specimens in (a) U loading direction, (b) V loading direction and (c) W loading direction. These specimens were prepared in Deviation 2 conditions

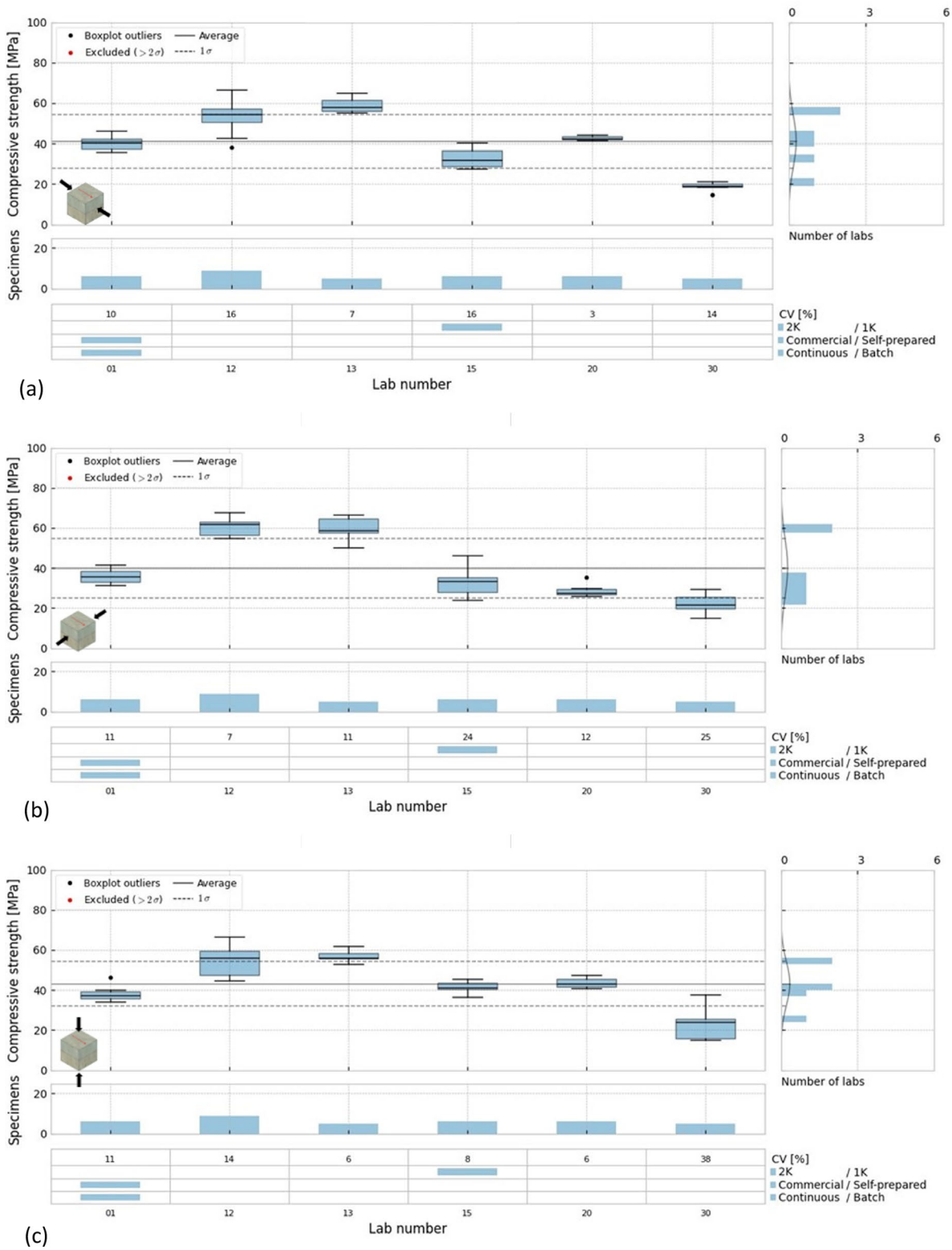


**Fig. 3** Compressive strength data reported by laboratories for mortar-scale printed specimens in (a) U loading direction, (b) V loading direction and (c) W loading direction. These specimens were prepared with cold joints (Deviation 1)

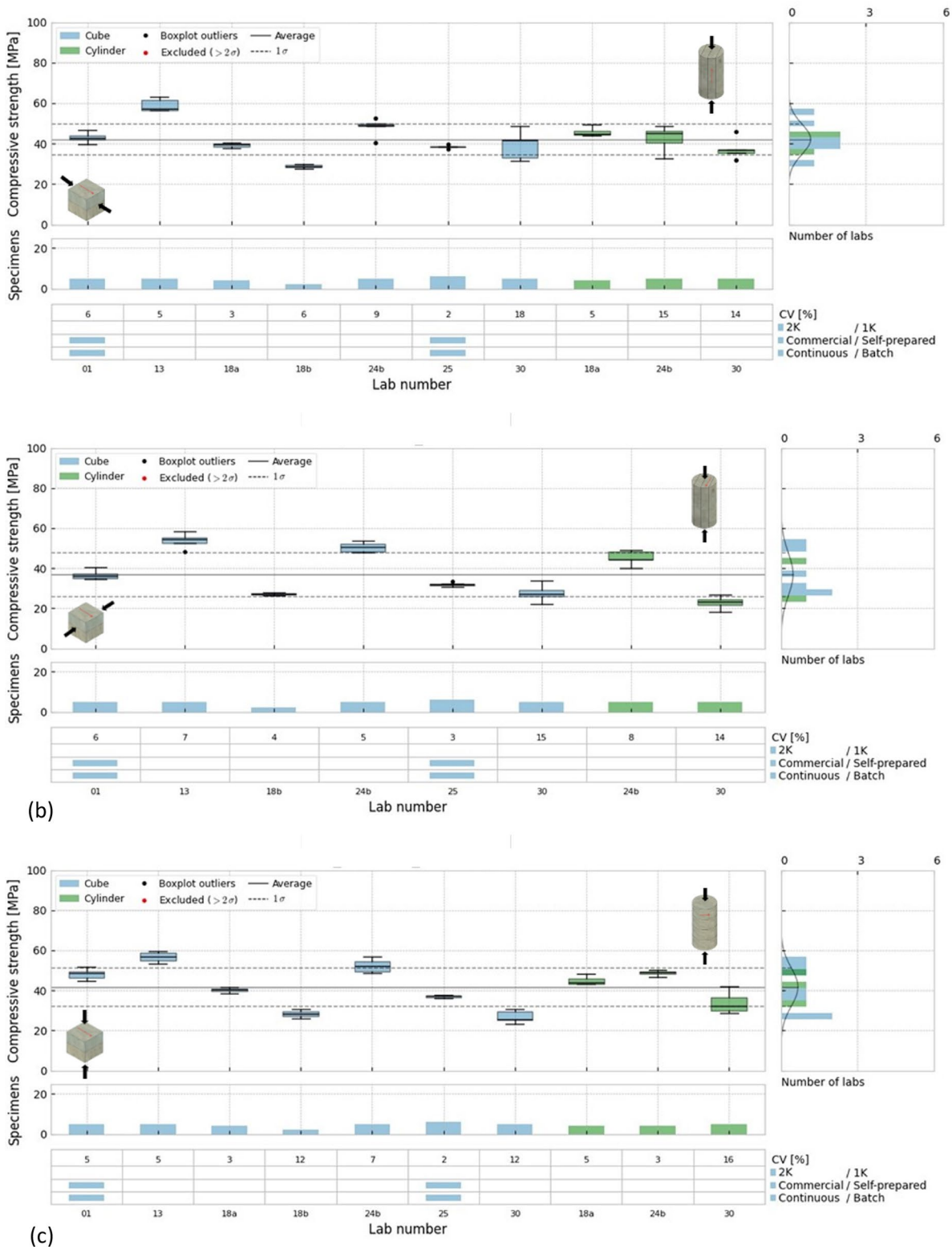


**Fig. 4** Compressive strength data reported by laboratories for concrete-scale printed specimens in (a) U loading direction, (b) V loading direction and (c) W loading direction. These specimens were prepared in Default conditions

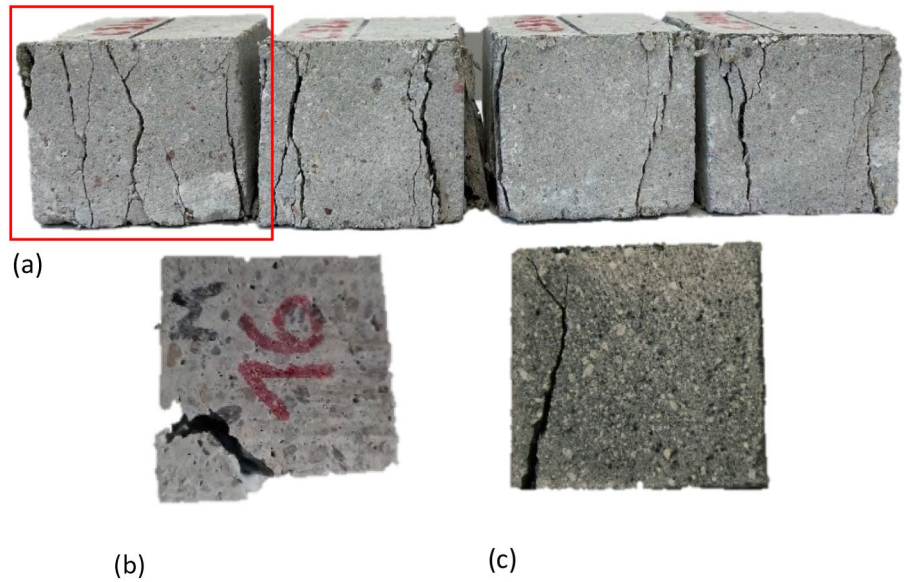


**Fig. 5** Crack patterns observed in printed cubes under compression for (a) Lab 11 in the U loading direction (side view), (b) Lab 04 in the V loading direction (top view), and (c) Lab 24 in the V loading direction (side view), highlighting premature failure, leading to scattering in the compressive strength data

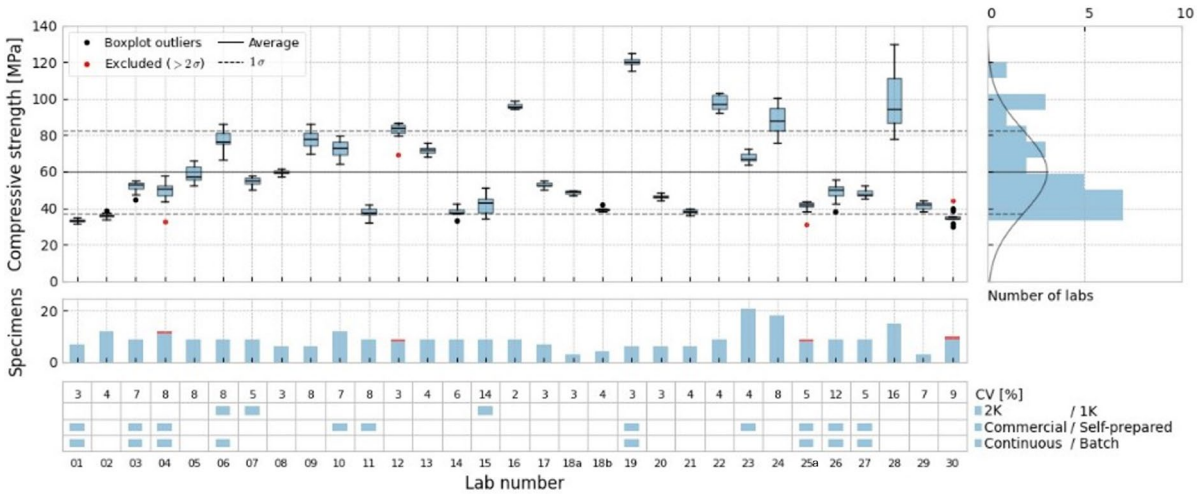


**Fig. 6** Compressive strength data reported by laboratories for mortar-scale cast specimens. These specimens were prepared with default conditions

of Lab 25a for the mortar-scale tests performed in the U-direction performed, Default conditions (Fig. 1a).

With regard to loading direction (Fig. 1), scattering was mostly higher in the V loading direction compared to the directions U and W. Printed specimens were typically weakest in the V direction, possibly because the interlayer defects are aligned along this loading direction. However, additional factors also contributed to the associated scattering. For instance, Lab 05 exhibited the highest scattering in the V loading direction (43% CV) compared to U (7% CV) and W (4% CV) loading directions. It was found that the scattering was also related to the extraction location of the specimens. The compressive strength of printed specimens extracted from the top, middle, and bottom sections were 29.9 MPa, 58.4 MPa, and 24.2 MPa, respectively, in V loading direction. For this laboratory, however, the extraction location did not significantly influence the U and W loading directions. In contrast, in some laboratories, the influence

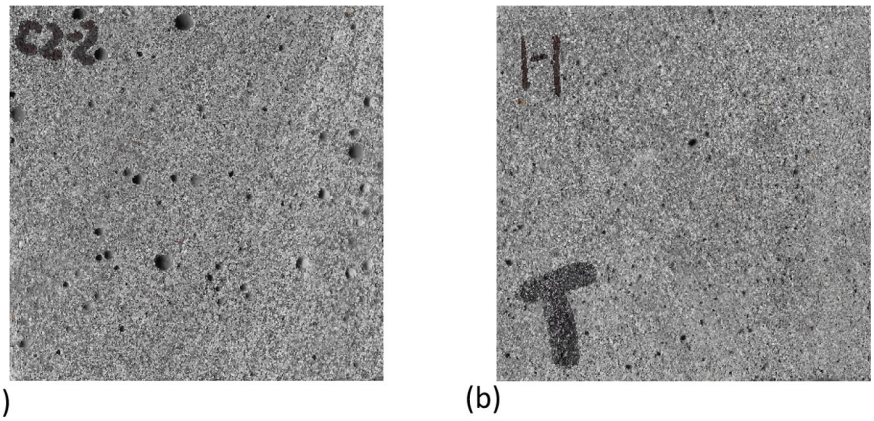


**Fig. 7** Cross section of (a) a cast and (b) a printed specimen used for the compressive strength testing by Lab 28

of extraction location on compressive strength was observed across the two loading directions. The effect of extraction location on compressive strength will be considered in more detail in the subsequent section.

Following the V loading direction, the scattering was observed to be most pronounced in U direction according to the average CV. Lab 04 exhibited the highest scattering in the U loading direction. Similar to the V direction, additional factors contributed to the scattering. For Lab 04, these were variations in the dimensions of the specimens used for testing. Specifically, both prisms (40 mm × 40 mm × 160 mm) and cube specimens (40 mm × 40 mm × 40 mm) were tested. Interestingly, the compressive strength values obtained from these prisms were 60% and 30% higher than those of the cubes in the U and W loading directions, respectively. Conversely, for cast specimens, the compressive strength of prisms was approximately 20% lower than that of cubes. The latter results is fully in line with our knowledge on the effect of the aspect ratio of the specimen on the compressive strength. Thus, the shift in trend from casting to 3D printing is notable indeed. Therefore, in subsequent sections, the average compressive strength for Lab 04 specimens was determined exclusively from cube specimens to avoid large scattering in the data. Similarly, in the W loading direction, the results from Lab 30 showed the highest scatter in cube specimens, as indicated by the coefficient of variation (CV), likely due to machine-related issues. This is supported by the lab's comments on faulty saw blades and low scatter observed in the cylindrical specimens which were extracted using a core-driller. Data points exceeding two standard deviations were excluded from further analysis.

Figure 2 shows that curing conditions also have a significant effect on the scattering of the data. When the curing conditions changed from Default to Deviation 2, some laboratories showed a notable shift in CV. For instance, in Lab 24, the CV was reduced from 13 to 5% in the U loading direction and from 19 to 4% in the V loading direction. Here, Deviation 2 signifies water bath for 90 days, in contrast to Default of 28 days water bath. While a lower CV is generally expected due to the higher concrete age, an interesting observation was made in the W loading direction. The CV increased from 10 to 14% with the increase in age. A similar trend was observed in other laboratories, such as Lab 05, Lab 06, Lab 13, and Lab 19, where the CV reduced in the U and V loading directions but increased in the W loading direction when curing conditions changes from Default to Deviation 2. In these cases, the concrete age remained similar to Default, but the curing was changed from water bath to ambient curing. Figure 3 presents the compressive strength data for printed specimens containing cold joints. These specimens were extracted from the middle section of the printed element, minimizing the influence of extraction location. Nevertheless, the data from various laboratories exhibited greater scatter compared to the Default specimens (without cold joints). Meanwhile, when the specimen size was changed from mortar-scale to concrete-scale, the CV among the compressive strength results decreased across all loading directions (Fig. 4). Despite the introduction of more interlayers in the concrete-scale specimens compared to the mortar specimens, the observed scatter was less pronounced. Overall, the observations suggest that factors such as extraction location,

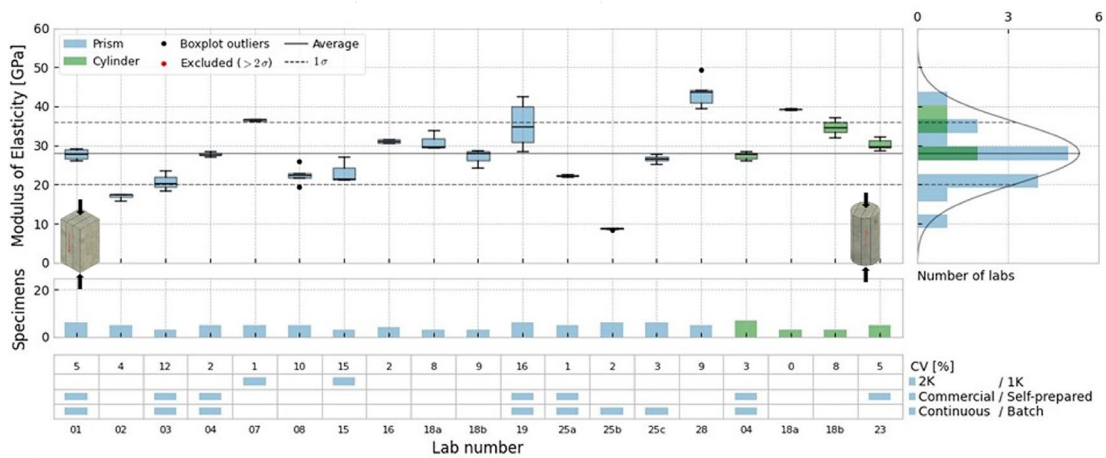


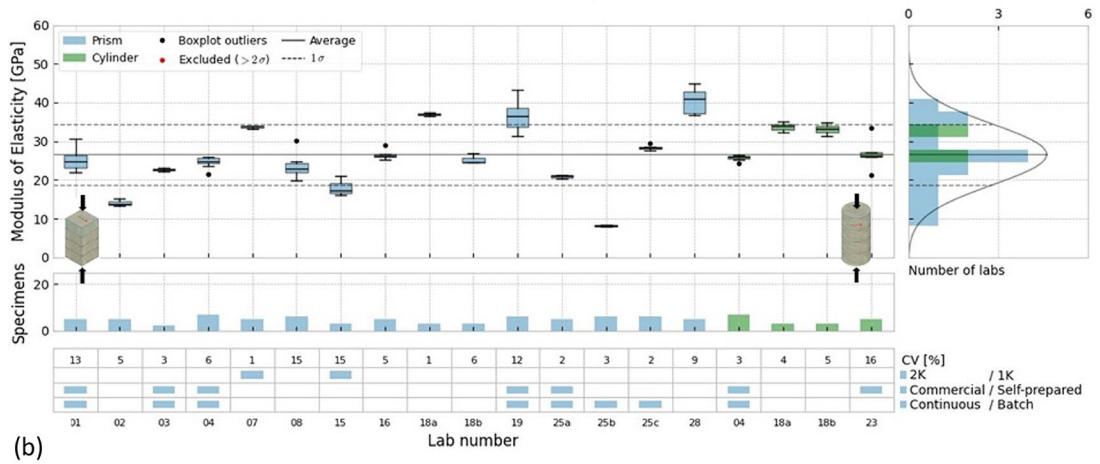


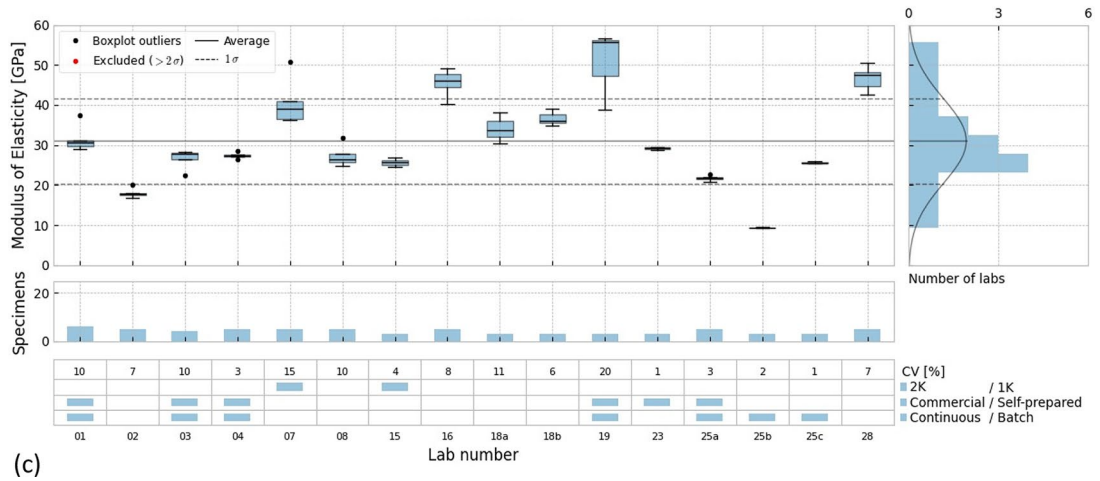


**Fig. 8** Modulus of elasticity data reported by laboratories for mortar-scale printed specimens in (a) U and (b) W loading directions and (c) cast specimens for default curing conditions

loading direction, specimen scale, cold joints, and curing conditions influence the compressive properties, as anticipated. Given that all laboratories adhered to uniform specimen preparation and testing procedures in this study, these parameters can now be analyzed in greater detail (Sects. 4.1–4.5).

### 3.2 Observations on compressive strength of cast specimens

Figure 6 shows the compressive strength data provided by labs for the cast specimens. The variation in observed compressive strength is attributed to the different mix designs used by individual laboratories. However, within each lab, the same mix design was used for both casting and printing specimens. In most cases, cast specimens exhibited higher compressive strength than printed specimens. However, in some cases, the opposite trend was observed depending on the loading direction, as shown in Fig. 12. The variation in compressive strength between cast and printed specimens, along with the influence of loading direction on this deviation, is discussed in detail in Sect. 4.2. This section also highlights specific labs that exhibited trends differing from the typical pattern. As anticipated, nearly all laboratories observed lower scattering in the compressive strength data for cast specimens compared to printed specimens. This is attributed to several factors, including the absence of interlayers and less processing of the specimens, such as grinding or capping before testing.

However, one lab measured a higher coefficient of variation (CV) for cast specimens compared to printed specimens. Namely, Lab 28 reported a CV of 4.6% for the U-direction, 11.8% for the V-direction, and 10.5% for the W-direction for printed specimens, but 15.7% for the cast specimens). It was found that the printable mix used for this study was very stiff, causing problems during casting. Figure 7a shows the cross-section of the cast specimen exhibiting a higher number of visible pores compared to the printed specimen (Fig. 7b), confirming improper compaction during casting. Meanwhile, during printing—depending on the rheological properties of the mixture—a superior compaction is provided through pumping and extrusion, which reduces the porosity of the printed layers. However, in majority of the labs, the porosity of the interlayers offsets this benefits, resulting in an overall increase in the porosity of the printed elements in comparison to the cast counterparts.

### 3.3 Observations on the modulus of elasticity data

Figure 8 shows the modulus of elasticity (MOE) for both printed and cast specimens obtained in this study. It was observed that the average MOE in the U direction was higher compared to the W loading direction. Additionally, similar to compressive strength, the average MOE for cast specimens exceeded that of printed specimens. While the trend of MOE across different laboratories followed a pattern similar to that of compressive strength, the relationship between MOE and compressive strength varied from lab to lab. Section 4.5 investigates this interrelationship in detail, emphasizing on the influence of the interlayers on the relationship between MOE and compressive strength.

With regard to scattering, the MOE exhibited lower CV values compared to the compressive strength data, as detailed in Sect. 3.1. Most likely it is due to the testing procedure. In the case of MOE, there are multiple checks during the tests that ensure the determined values are reliable and repetitive [6]. Regardless, there are a few labs that reported high scattering in the modulus of elasticity data. The highest scattering was observed by Lab 19, with a CV of 14.9% in U loading direction, 10.7% in W loading direction, and 16% in cast specimens. No clear reason for this behavior could be identified. It is worth mentioning that the compressive strength data from Lab 19 also showed high scatter (see Fig. 1). Overall, no data points exceeded the 2-standard-deviations-thresholds, allowing for the inclusion of all data points in the further investigation.

## 4 Discussion of the results

This section evaluates the test results selected from prior observations by correlating two sets of data points at a time. The data points are the average compressive strength or modulus of elasticity values of laboratory-material series determined for a specific parameter variation such as mortar-scale-default curing and U loading direction. Initially, a linear regression is calculated between the two sets of data points. Cook's distance (D) is then computed for each data

point and any point with D > 1.0, indicating a significant influence on the quality of the linear regression, is excluded from further analysis. The linear regression is then recalculated for the remaining data points, and any point exceeding two standard deviations is also removed. The data points that are removed based on Cook's distance and two standard deviations are clearly marked on the corresponding graphs used for visualization. For the remaining data points, a linear best fit through the origin is computed, assuming proportionality and zero intercept between the two data sets. The statistical parameters derived from this fit include k, representing the ratio between the data sets, $R_0^2$, indicating the degree of correlation and $\sigma$ representing the standard deviation. Additionally, a best fit line without assuming a zero intercept is also plotted using a dashed blue line. The correlation degree for this fit is provided as $R_i^2$ in the graphs. This methodology for correlation and outlier exclusion is applied consistently throughout the results and discussion section except for Sect. 4.5, where the relationship between MOE and compressive strength is non-linear.

### 4.1 Influence of extraction location on compressive strength

In Sect. 3.1, the scattering in compressive strength data of various labs was attributed to the extraction location. Consequently, this section investigates whether the extraction location significantly impacts the results across all 30 laboratories. This was achieved by correlating the average compressive strength of printed specimens from each extraction location (bottom, middle, and top) with the bulk average compressive strength. The term "bulk" refers to scenario where the average was calculated using all specimens regardless of the extraction location. The outliers identified in the previous section were reassessed for the objective of this section. For instance, Lab 12 reported nine values of compressive strength under the U loading direction and default curing conditions. Among these, one value was previously identified as an outlier. However, in this section, the data from Lab 12 was further categorized based on the extraction location, resulting in three datasets: bottom, middle, and top. When the 2STD (two standard deviations) method was applied to these subcategories (as explained in Sect. 3), the value was no longer identified as an outlier. More than 10 laboratories in each loading direction showcased similar particularities. To investigate if the previously identified outliers need reassessment for correlating extraction location and bulk compressive strength, two approaches were used:

1. No outliers removed: The average compressive strength is calculated using all submitted data from the laboratories without excluding the outliers identified in the previous section.
2. Outliers removed in both: The average compressive strength is calculated for both the bulk data and the extraction location data after excluding the outliers.

As shown in Figs. 9 and 10, under Default curing conditions, eliminating the outliers identified in the previous section led to a slight enhancement in the correlation. Therefore, further analysis utilized the approach where outliers were removed from both the bulk and extraction location datasets. Regardless of the loading direction and extraction location, the compressive strength from specific locations (top, middle, and bottom) were similar to the bulk strength. However, some laboratories exhibited contrary results. For instance, Lab 05 showed a significant reduction in compressive strength in the V loading direction. This reduction was particularly evident in specimens extracted from the top and bottom sections of the printed wall. When specimens were extracted from the middle section of the printed wall, the compressive strength was similar across all the loading directions. The average compressive strength for Lab 05 for specimens loaded in the V direction and extracted from the top, middle, and bottom locations was 29.96 MPa, 58.40 MPa, and 24.22 MPa, respectively. The middle section exhibited more than twice the strength compared to the other two extraction locations, leading to the lab being an outlier in all three extraction locations. Meanwhile, the effect of extraction location was insignificant in the U and W loading directions. The average compressive strength of specimens extracted from the middle section was approximately 10% higher than those from the top section and 5% higher than those from the bottom section, for both U and W loading directions. Similarly, the cylindrical specimens from Lab 15 exhibited significant deviations from the average trend in the V-loading direction for both the top and bottom

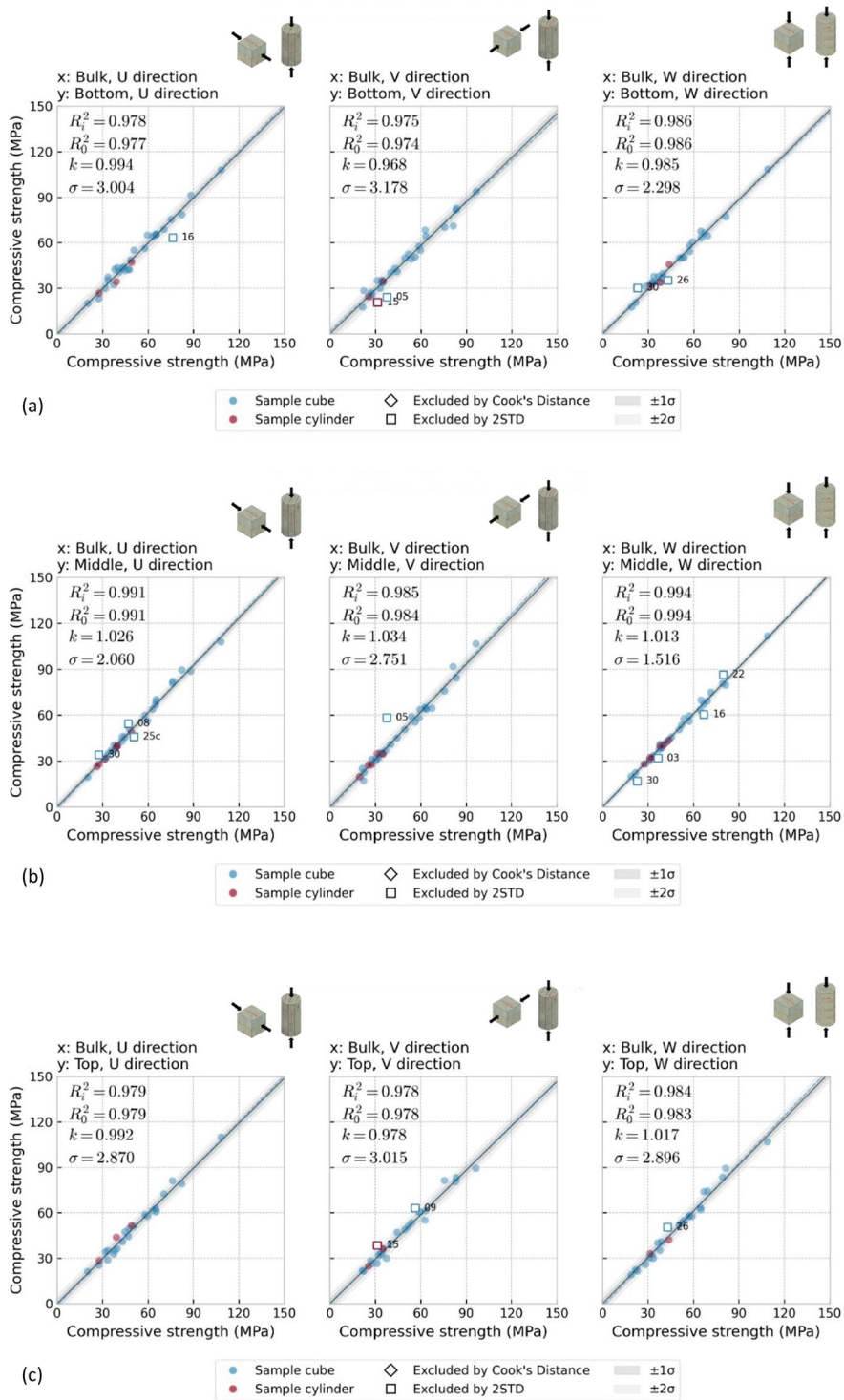


**Fig. 9** Correlating average compressive strength of mortar-scale specimens extracted from (a) bottom (b) middle and (c) top sections of the printed element to the average bulk compressive strength. No outliers were removed while determining the respective average compressive strengths. Images from left to right represent U, V, and W loading directions

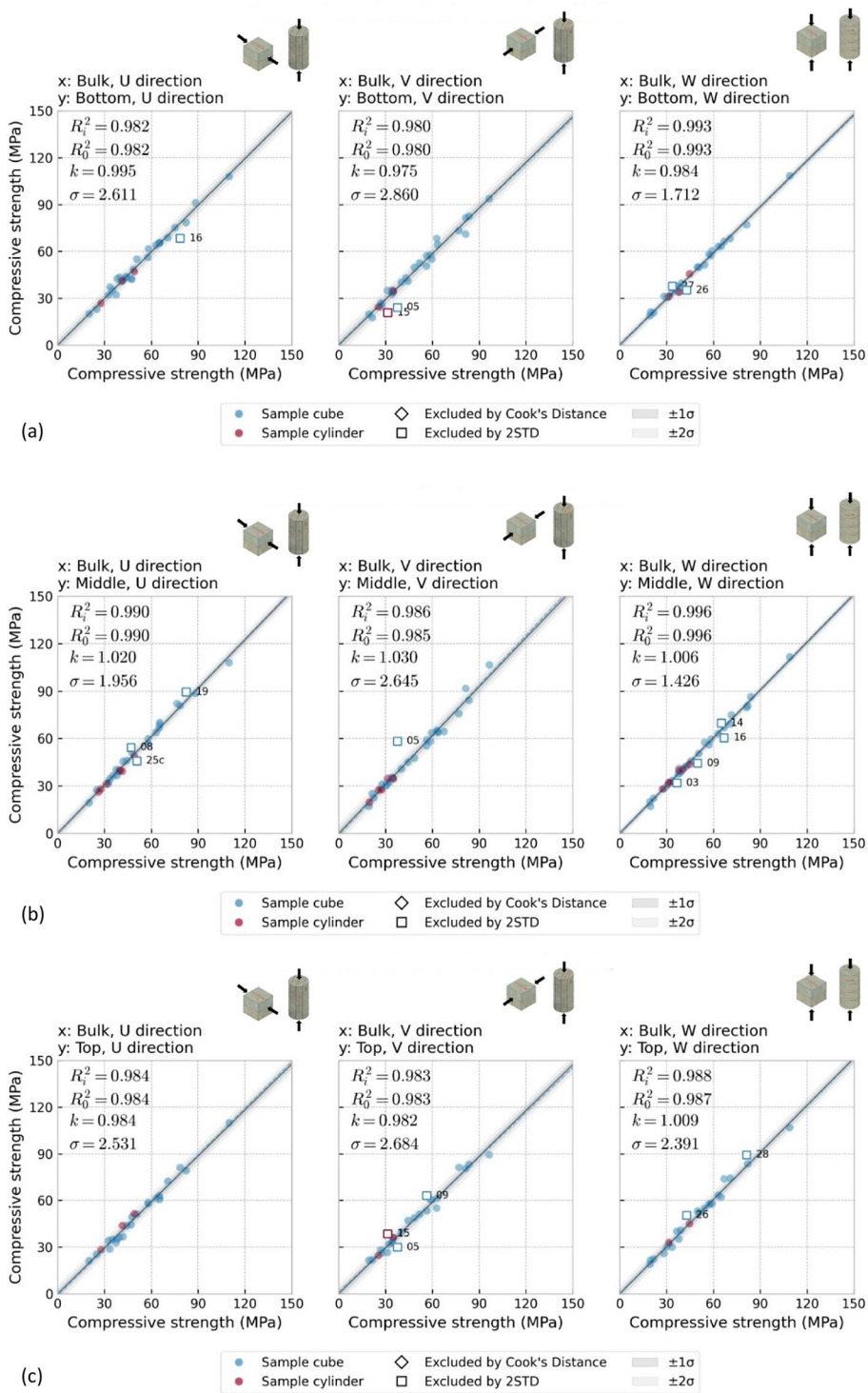


**Fig. 10** Correlating average compressive strength of mortar-scale specimens extracted from (a) bottom (b) middle and (c) top sections of the printed element to the average bulk compressive strength. Outliers were removed while determining the respective average compressive strengths. Images from left to right represent U, V, and W loading directions


**Fig. 11** Print beds used by **a** Lab 26 and **b** Lab 16

extraction locations. However, for Lab 15, the average compressive strength for the bottom extraction location was the lowest, but the strongest specimen was from the top instead of the middle extraction location, as seen in Lab 05. Additionally, the cube specimens of Lab 15 showed no significant influence of extraction location on the compressive strength.

There were also several laboratories that showed significant deviation from the average trend in U and W loading directions. For example, Lab 26 in the W loading direction reported average strengths of 35.27 MPa, 42.52 MPa, and 50.57 MPa for the bottom, middle, and top extraction locations, respectively. As a result, Lab 26 was excluded from the analysis based on a 2STD-criterion for both the top and bottom extraction locations. In this lab, the compressive strength was consistently the lowest for the bottom specimens across all loading directions. This suggests the presence of defects specific to the bottom section of the printed element. Figure 11a provided by Lab 26 indicates that the printing was done on a dry platform, potentially resulting in higher moisture loss in the bottom layers, thereby leading to lower strength values. Similarly, Lab 16 displayed significantly lower compressive strength in the bottom section under the U loading direction, marking it as an outlier. However, the bottom specimens did not exhibit the lowest strength in the other two loading directions. Interestingly, in the W loading direction, the lowest compressive strength was found in the middle section instead. Figure 11b provided by this lab shows that printing was not performed on a dry platform as in Lab 26, resulting in the bottom specimens not consistently showing the lowest compressive strength. Unlike Lab 16 and Lab 26, the compressive strength for Lab 27 was consistently the highest when specimens were extracted from the bottom section for all loading directions. Moreover, the top specimens consistently exhibited the lowest compressive strength. Further investigation revealed that the printing was conducted under conditions where the relative humidity (RH) was approximately 20%. Therefore, it is likely for the printed object to lose moisture to the surroundings, with top layers being more susceptible to this effect, which could possibly explain the observation. Additionally, low RH could lead to a faster stiffening of fresh mixture, worsening its extrudability and interlayer bonding while printing the top layers, eventually reducing the compressive strength of the top section.

Overall, the correlation in compressive strength was better for the W loading direction across all extraction locations compared to the U and V loading directions. This is expected, as deviations associated with interlayers are more pronounced in the U and V directions. Additionally, within the W loading direction, specimens extracted from the middle section showed the best correlation. This resulted in more laboratories falling beyond the 2STD-threshold for this combination, leading to the exclusion of four laboratories from the analysis. The deviation in compressive strength values for these laboratories was minimal compared to those excluded in the U and V loading directions, so a further investigation was deemed unnecessary.

### 4.2 Comparison between compressive strength of printed and cast specimens

Figure 12 illustrates the relationship between the average compressive strength of printed specimens in each loading direction and that of the cast specimens. Only mortar-scale cube specimens were utilized for this analysis, as the numbers specimens of other shapes and sizes were insufficient to perform a reliable correlation. Based on the findings from the previous section, the compressive strength of printed specimens was calculated by averaging the compressive strength values of specimens from all extraction

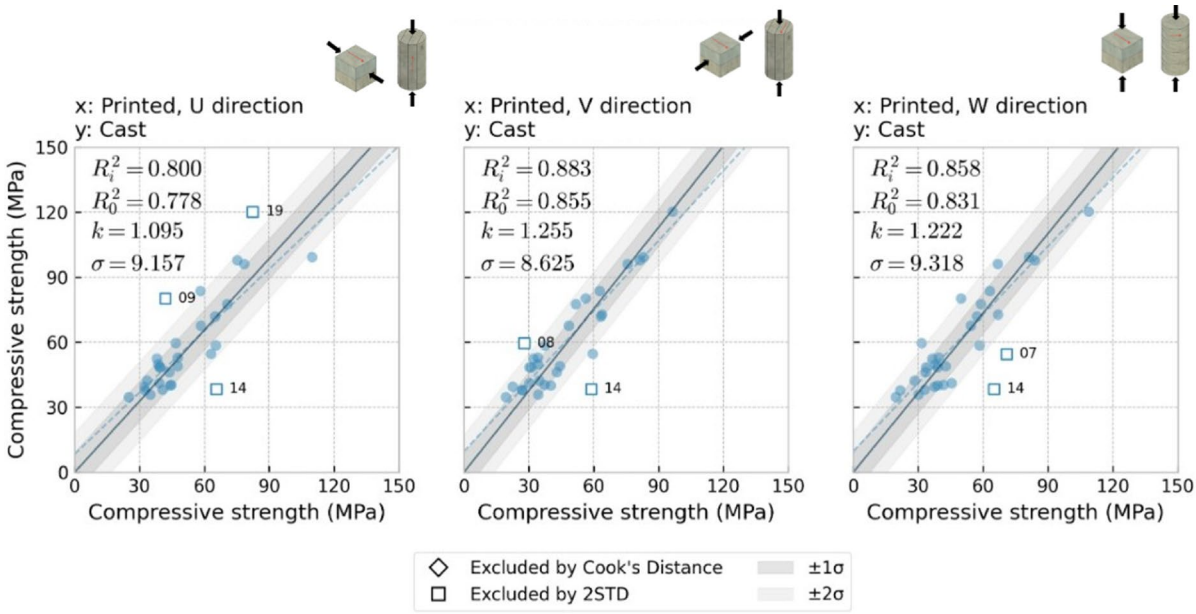


**Fig. 12** Correlating compressive strength of mortar-scale printed specimens to the cast specimens. These specimens were prepared under Default curing conditions. Images from left to right represent U, V, and W loading directions

locations (bulk dataset). The data was not subdivided into different extraction locations.

The compressive strength of printed specimens exhibited a fairly good correlation with that of cast specimens. Notably, the correlation was stronger for the V and W loading directions compared to the U loading direction. Approximately 25% of printed specimens in the U loading direction exhibited higher strength than the cast specimens. However, this behavior was less evident in the V and W loading directions, where only 5% of the laboratories showed printed specimens exhibiting higher strength than the cast specimens. This led to a better correlation in these two loading directions. Overall, the printed specimens showed lower compressive strength than cast specimens, with the U loading direction showing the least reduction in strength at 8.7%, compared to 18.2% and 20.3% for the W and V loading directions, respectively. This highlights the anisotropic nature of 3D-printed concrete.

Contrary to the average trend, some laboratories reported significantly lower compressive strength for printed specimens compared to cast specimens in the U loading direction. For example, Lab 19 showed approximately 30% lower 28-day strength in the U loading direction compared to its cast specimens, identifying it as an outlier. Additionally, printed specimens in the U loading direction displayed lower strength than those in the other two loading directions, which deviates from the general trend. However, the 7-day compressive strength measurements of Lab 19, which were taken to address the discrepancy observed at 28 days, indicated that the U loading direction had higher strength than the other two loading directions, aligning with the overall trend. Furthermore, it was observed that the 28-day compressive strength of printed specimens in the U loading direction was lower than the strength at 7 days, whereas the compressive strength for the V and W loading directions increased over the same period. This suggests that the lower 28-day compressive strength in the U loading direction may have been due to faulty specimens or testing procedures. As a result, this data point was justified as an outlier and excluded from the analysis.

In contrast, Lab 14 exhibited significantly higher compressive strength for printed specimens compared to cast ones. In the U, V, and W loading directions, the printed specimens yielded 70%, 53%, and 68% higher values of the compressive strength than those measured on the cast specimens, respectively, resulting in the lab being an outlier for all three loading directions. To confirm this contradictory observation, the cast

specimens were prepared again and tested by Lab 14; however, the trend remained the same. Most likely, this discrepancy is related to the rheological properties of the mix used. The spread diameter (according to [14]) and static yield stress of the mix were determined as 160 mm and 1600 Pa, respectively, indicating a stiff mix that likely led to low compaction during casting. This assessment was corroborated by visual observations made by the lab members. In the case of printing, the material was pumped using a progressive cavity pump to a hopper, which provided significant compaction. Additionally, the concrete in the hopper was vibrated with a poker vibrator to attain the rheological properties required for smooth extrusion. The compaction was further enhanced in the nozzle region, where concrete was "reshaped" to print a 50 mm × 20 mm filament from a pumping hose of 25 mm diameter. The rectangular nozzle ensured the printed specimens had the required dimensions without the need for additional horizontally adjacent filaments, unlike in many other laboratories. Moreover, a vertical layer offset of 16 mm ensured sufficient interlocking between the vertical layers. This combination of factors justifies why the printed specimens exhibited higher strength than the cast specimens.

A high static yield stress mix exhibiting higher compressive strength for printed specimens than for the cast specimens was expected to be common in the multiple-component system. Interestingly, only one lab out of three that used multiple-component mixes reported such behavior. For Lab 07, the printed specimens showed 15% and 9% higher strength than the cast specimens in the U and V printing directions, respectively. Meanwhile, in the W loading direction, the printed specimens showed 30% higher compressive strength than the cast specimens, causing the results to be an outlier in this loading direction. The mix used by Lab 07 for printing had a static yield stress of 1380 Pa, suggesting the mix to be quite stiff, which may cause insufficient compaction while casting. Moreover, preparing cast specimens from multicomponent mixes is challenging due to both the high static yield stress and inadequate vibration during compaction. Unlike single-component mixes, multicomponent mixes are typically deposited into molds from the nozzle of the printer, i.e., after print head mixing. The printer is often located far from the conventional vibration table used for compacting fresh specimens. As a result, concrete may begin setting before reaching the vibration table, potentially causing defects and reducing strength compared to printed specimens. Although the labs have used alternative compaction methods to avoid transporting the concrete-filled molds to a distant vibration table, these methods are generally less effective than the vibration tables used for single-component mixes.

It can be observed that the compressive strength of cast specimens correlates to that of printed specimens, as the $R_0^2$ values appear to be within acceptable limits for concrete mechanical properties. However, it should be noted that with the current knowledge it is not possible a-priori to define where a certain material composition or printing system is positioned, or even whether it would fall in- or outside of the outlier criteria applied here. A high initial static yield stress or rapid setting rate seems to indicate behavior deviating from the average (due to a lack of compaction in cast specimens). However, this does not explain all outlier results. Therefore, these correlations cannot be used to determine engineering properties of a given material-printer combination without further consideration. This will be subject of future work of the RILEM TC 304-ADC.

### 4.3 Effect of scale factor on the compressive strength

In the last two sections, only mortar-scale specimens will be addressed. However, the scale of the specimen likely affects the compressive strength due to the presence of additional interlayers. Since the dimensions of the printed layers are consistent across both mortar-scale and concrete-scale specimens, printing concrete-scale specimens will result in more interlayers compared to the mortar-scale specimens. Therefore, this section examines the effect of scale factor on the compressive strength. Laboratories that conducted compressive strength tests on both concrete-scale and mortar-scale specimens under similar printing and curing conditions were analysed. The only variable is the size of the specimens. Laboratories using two different mix designs for mortar-scale and concrete-scale specimens were excluded. Likewise, results were omitted from the analysis if the age difference between the specimens exceeded three days.

Figure 13 presents a comparison between mortar-scale and concrete-scale specimens in three loading directions. It was found that the compressive strength of concrete-scale cube-shaped specimens was generally similar to, or lower than that of the mortar-scale

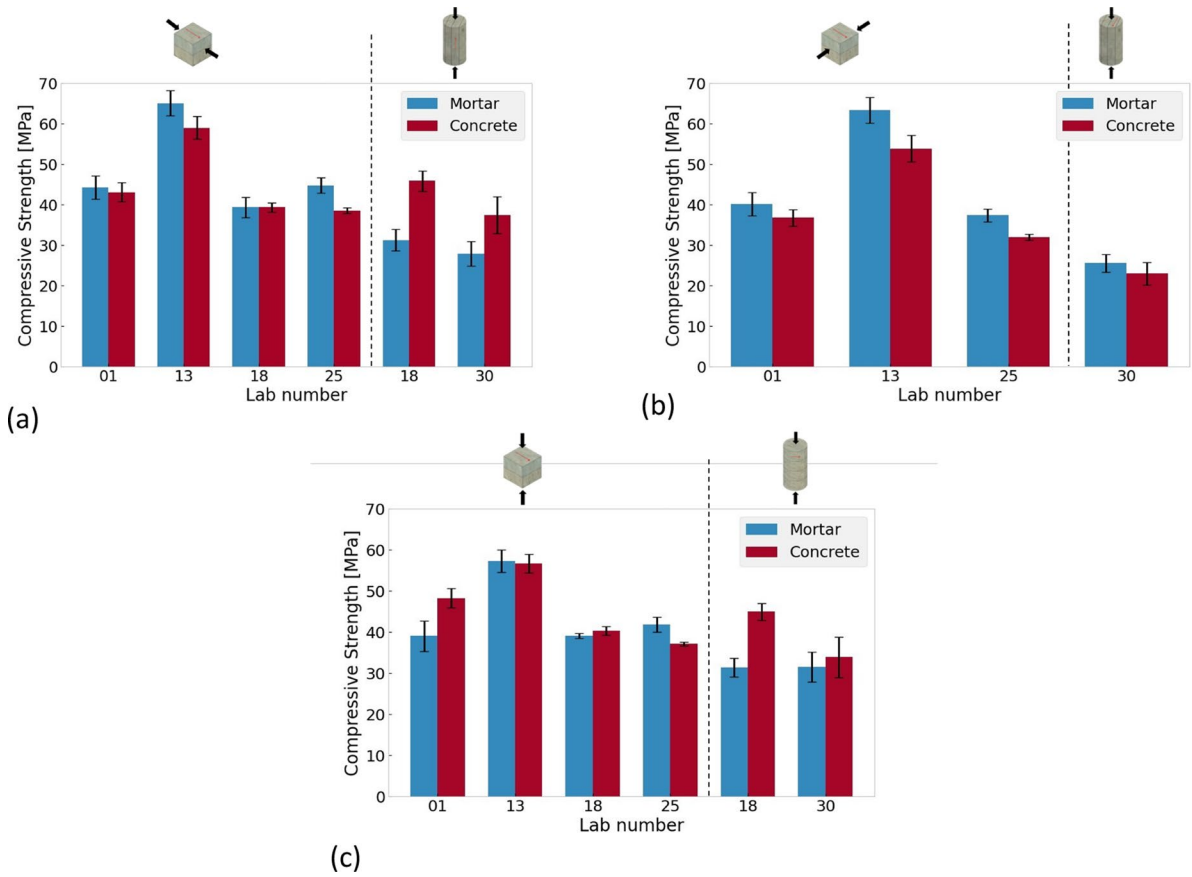


**Fig. 13** Comparing compressive strength of mortar-scale printed specimens to the concrete-scale printed specimens in (a) U loading direction, (b) V loading direction and (c) W loading direction. These specimens were prepared under default curing conditions

specimens across most laboratories, regardless of the loading direction. This trend is consistent with the findings reported in [15] for cast specimens, where compressive strength tends to decrease as specimen size increases.

The reduction in compressive strength was substantial in the U and V loading directions compared to the W loading direction. For example, Lab 13 showed approximately a 10% and 15% decrease in compressive strength in the U and V loading directions, respectively, when the specimen size was increased from the mortar-scale to the concrete-scale. In contrast, the compressive strength difference between mortar-scale and concrete-scale specimens in W loading direction was insignificant. This trend was consistent across multiple laboratories, except in Lab 01, where the compressive strength of concrete-scale specimens was higher than that of mortar in W loading direction. Concrete-scale specimens, unlike their mortar counterparts, contain vertical interfaces resulting from multiple horizontal layers printed to attain the required dimensions. These additional interfaces should decrease the compressive strength of concrete-scale specimens compared to mortar counterparts in W loading direction. However, for Lab 01, it was found that it exhibited a shift in anisotropic behavior when the specimen size was increased from the mortar-scale to the concrete-scale. The mortar-scale specimens yielded the lowest compressive strength in the W loading direction compared to the U and V directions. However, for concrete-scale specimens, the W loading direction exhibited the highest compressive strength. To illustrate with values, the compressive strength of mortar-scale specimens in the U, V, and W directions was 44.23 MPa, 40.21 MPa, and 39.05 MPa, respectively.

When the scale was increased to that of concrete, the compressive strength in the U, V, and W directions was 43.05 MPa, 36.76 MPa, and 48.20 MPa, respectively. This shift in anisotropy in Lab 01 caused the concrete-scale specimens to have higher strength than their mortar counterparts in the W loading direction. A similar shift in anisotropy was also observed in Lab 13, although to a lesser extent, resulting in mortar-scale and concrete-scale specimens exhibiting similar compressive strengths in the W loading direction.

However, in the other two laboratories, the W loading direction did not show similar effect from the change in scale factor. In the case of Lab 18, neither scale factor nor loading direction changed the compressive strength of the printed specimen, possibly due to the variation in printing strategy compared to other laboratories. A slab of 750 mm×750 mm cross section was printed from which both the mortar and concrete-scale specimens were extracted for the analysis. The vertical and horizontal offset used for this printing ensured significant merging of the layers. As a result, the printed slab most likely behaved like a cast specimen which could be associated to the minimal variation in compressive strength across different loading directions and scales. On the other hand, Lab 25 showed an influence of scale factor on the compressive strength, but anisotropic behavior was similar for both mortar and concrete-scale specimens. In both scales, the loading direction V showed the lowest compressive strength. The printing parameter and specimen preparation were similar to lab to 1 and 13. Nevertheless, the shift in anisotropy was not noticed in this lab when the scale was increased from mortar to concrete. This implies that the results are not sufficient to draw a definitive conclusion about the effect of scale on the shift in anisotropy. However, in theory, due to the presence of additional interfaces, concrete-scale specimens should exhibit lower strength compared to mortar-scale specimens without deviating in their anisotropic behavior. Lab 01 is most likely an exception.

When the specimen shape was changed from cube to cylinder, the compressive strength of concrete-scale specimens was found to be similar to or higher than that of mortar-scale specimens. This contradicts the trend observed in cube specimens (both printed and cast [15]) and is likely attributed to the specimen extraction method. Since core drilling was used to extract cylindrical specimens, the extensive energy exerted during the core-drilling process might have affected a smaller volume in the mortar-scale specimens to a higher extent compared to the concrete-scale specimens. As a result, mortar-scale specimens are likely to be more vulnerable to damage during extraction, leading to a lower compressive strength. This hypothesis is supported by data from Lab 18, where the compressive strength of concrete-scale specimens increased, while the compressive strength of mortar-scale specimens decreased substantially when the extraction method was changed from sawing (for cubes) to core-drilling (for cylinders).

Overall, it can be concluded that increasing the scale of cube-shaped specimens from mortar to concrete results in a slight reduction in compressive strength, likely due to the presence of additional interlayers. This reduction is more pronounced in the U and V loading directions compared to the W loading direction. Although one lab reported higher strength in the W loading direction when scaling up from mortar to concrete, the limited data makes it difficult to draw definitive conclusions. Additionally, it was found that the extraction method (sawing or core-drilling) plays a crucial role and should be carefully considered in relation to the specimen scale when characterizing the compressive strength of printed elements.

### 4.4 Effect of cold joint (Dev 1) and curing condition (Dev 2) on the compressive strength

In large-scale construction, it is likely that the delayed stacking of layers due to long print path causes cold joint between the layers. Thus, understanding the impact of cold joints on the performance of the printed structure is crucial. This section examines the influence of cold joints on compressive strength by comparing the average compressive strength of printed specimens produced under Default conditions (without cold joints) and Deviation 1 conditions (with cold joints). For this correlation, only specimens from the middle section were considered for the default condition, as the cold joint data (Deviation 1) was obtained solely from the middle section of the printed elements.

Figure 14 shows the correlation between the compressive strength of printed specimens with and without cold joints. Overall, it was found that the effect of cold joints was prominent in the U and V loading directions, which are relatively more sensitive

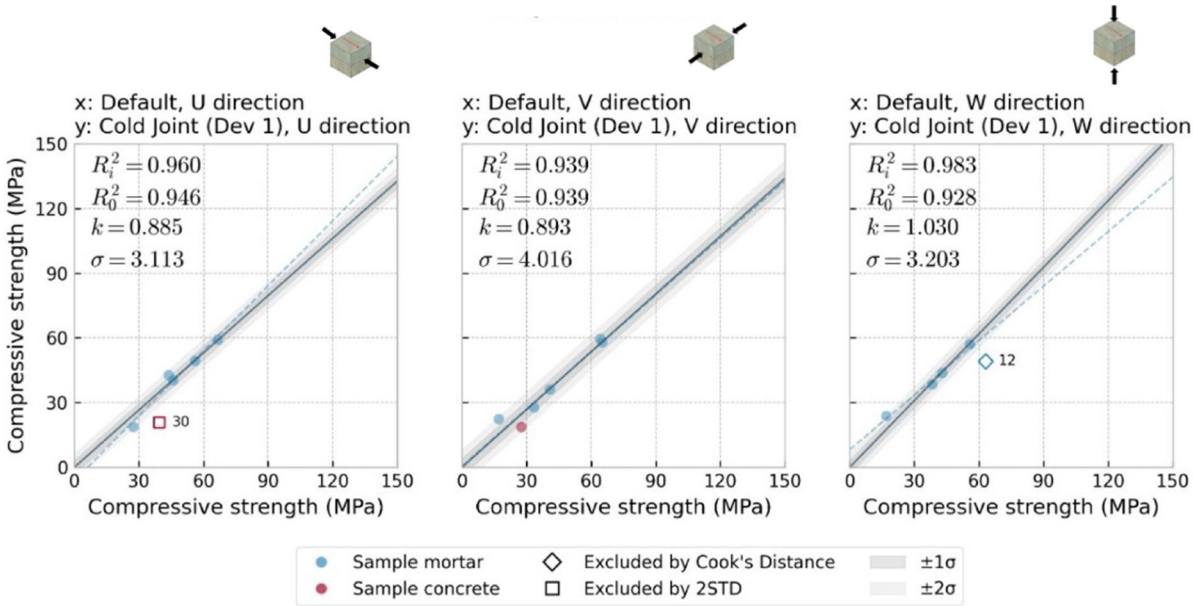


**Fig. 14** Correlating compressive strength of mortar-scale printed specimens with cold joints to the specimens without cold joints. Images from left to right represent U, V and W loading direction

to the interlayers compared to the W loading direction. In the U and V loading directions, the printed specimens with cold joints showed lower strength than those without, with a reduction of approximately 10%, whereas the effect of cold joints was found to be negligible for the W loading direction. However, in the case of Lab 30, a notable exception was observed. The compressive strength of specimens prepared with cold joints was significantly higher (~40%) than that of the specimens without cold joints when loaded in the V and W loading directions. This contradiction arises from the difficulties encountered by this lab during the extraction and preparation of printed specimens, as pointed out in Sect. 3.1. These challenges led to eccentric loading and premature failure of printed specimens without cold joints. The lab members have confirmed that the extraction process was subsequently improved, resulting in specimens with cold joints not experiencing the same issues. This conclusion is reinforced by the findings from concrete-scale specimens tested by Lab 30, which revealed lower compressive strength in printed specimens with cold joints compared to those without cold joints. Nevertheless, Lab 30 was retained for analysis, as the relationship was not statistically deemed an outlier. In contrast, Lab 12 was identified as an outlier in the W loading direction based on Cook's distance. The compressive strength of specimens with cold joints was found to be approximately 20% lower than the default, while the overall correlation showed insignificant change. Notably, the reduction in compressive strength was most pronounced in the W loading direction, which theoretically should be the least sensitive direction to cold joints. No attributable reasons were identified for this behavior from the available information.

Another significant factor in construction is the curing conditions. While the compressive strength values discussed in previous sections were obtained from water-bath curing, this method does not accurately represent the hardening behavior of large-scale printed elements. To better simulate the conditions during large-scale construction, the printed specimens were cured under ambient conditions (Deviation 2). These were then compared to the printed specimens cured in a water bath (Default), as shown in Fig. 15. Since the laboratories had the freedom to choose their Deviation 2 conditions, two laboratories opted for steam curing and extended concrete age (91 days in water bath) respectively as the Deviation 2 conditions. As these conditions do not align with the goal of the analysis, these two laboratories were excluded for this section.

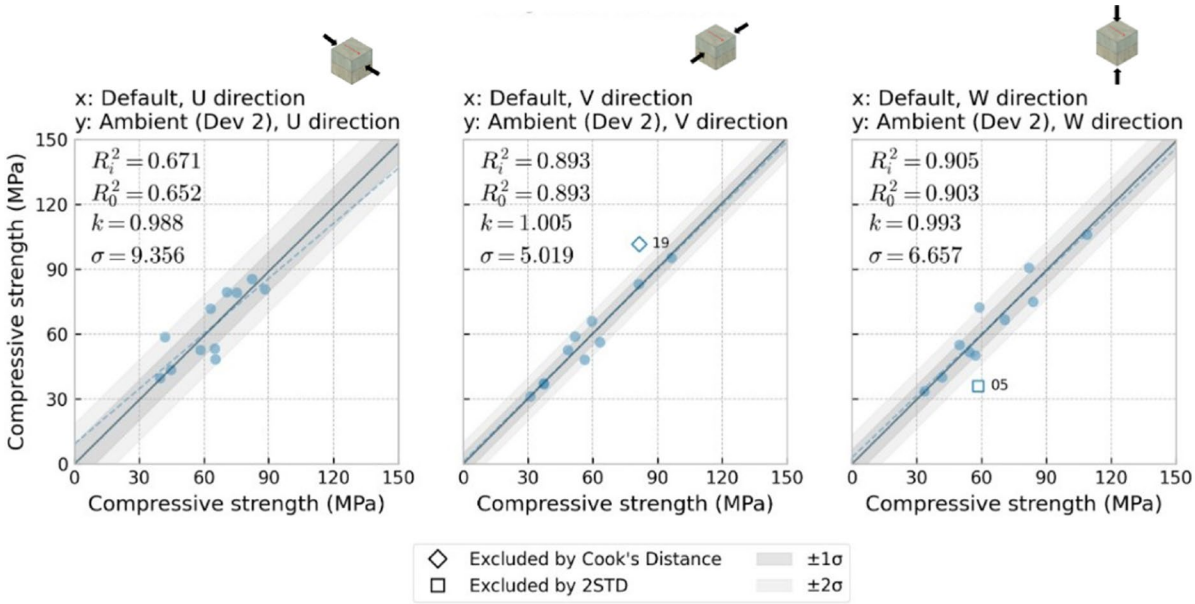


**Fig. 15** Correlating compressive strength of mortar-scale printed specimens cured in water bath to specimens cured in ambient condition. Images from left to right represent U, V and W loading direction

The temperature and relative humidity during ambient curing conditions (Dev 2) varied between 17 °C–23 °C and 35%–65%, respectively, across the laboratories. Despite these variations, the correlation between compressive strengths under two different curing conditions was notably strong in the V and W loading directions but comparatively weaker in the U loading direction. In the U loading direction, an approximately equal number of laboratories reported higher strength under water bath curing conditions compared to ambient curing conditions, and vice versa, causing weaker correlation. The highest decrease in compressive strength (26%) from water bath to ambient curing conditions was observed in Lab 05 under U loading direction. In Lab 05, the curing temperature remained nearly same, but the relative humidity was 65% for ambient curing compared to 100% for the water bath. Despite other laboratories experiencing greater difference in relative humidity, they showed smaller decreases in strength compared to Lab 05, suggesting that relative humidity alone was not the sole factor. The printable mix used by Lab 05 contained 50 wt% of the binder as slag, known for its slow early-age hardening properties. Consequently, when the printed elements were exposed to ambient conditions with lower humidity, the slow early-age hardening caused enhanced moisture loss from the specimens. This led to higher reduction in compressive strength under ambient curing conditions than water bath. The equally significant reduction in the compressive strength observed in other loading directions corroborates the hypothesis.

In contrast, some laboratories demonstrated an increase in compressive strength when the curing conditions were changed from water bath to ambient. Lab 09 showed the highest increment of approximately 40%. Under water bath, Lab 09 achieved average compressive strengths of 41.93 MPa, 56.38 MPa, and 49.89 MPa in the U, V, and W loading directions, respectively. However, under ambient curing conditions, the compressive strengths were 58.65 MPa, 48.14 MPa, and 55.06 MPa in the U, V, and W loading directions, respectively. This indicates that the increase in strength was primarily observed in the U and W loading directions. In contrast, the V loading direction showed a reduction in compressive strength. Interestingly, while the V loading direction exhibited the highest strength under water bath curing conditions, it showed the lowest strength under ambient curing conditions. Similar shifts in anisotropy were also observed in 4 out of 10 laboratories when the curing conditions were changed. This variability

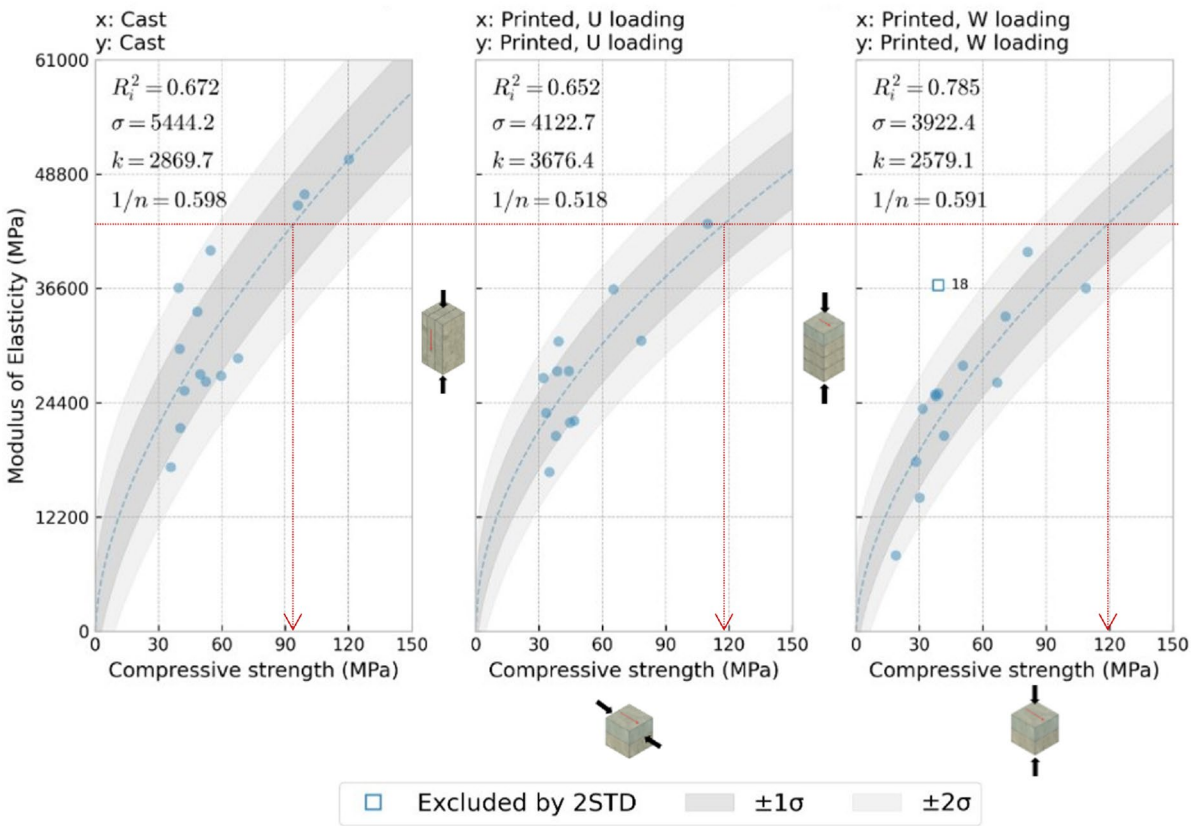


**Fig. 16** Correlating modulus of elasticity (MOE) with compressive strength of mortar-scale specimens prepared in Default condition. Images from left to right represent cast specimens and printed specimens tested in U and W loading direction. The MOE and compressive strength were determined using separate specimens

suggests that under water bath curing, compressive strength can either increase or decrease compared to ambient curing depending on the loading direction.

Based on these findings, curing conditions appear to influence the anisotropy in printed specimens. However, there is significant variation in the ambient curing conditions used by different laboratories, and only half of the laboratories showed a noticeable shift in anisotropy. Therefore, further assessment is necessary to draw definitive conclusions. Furthermore, the data suggests that compressive strength obtained from standard water-bath curing can be reasonably correlated with compressive strength obtained from ambient curing, particularly in the V and W loading directions. Nonetheless, it's important to exercise caution when dealing with mixes that are sensitive to surrounding humidity, as this factor can have a substantial impact on the results.

### 4.5 Influence of 3DCP on the relationship between MOE and compressive strength

The *fib* Model Code 2020 (MC 2020) relates the modulus of elasticity (MOE) and compressive strength of concrete using Eq. 1, where E is MOE in MPa, $f_c$ is compressive strength in MPa, k is a coefficient that depends on the type of aggregate used in the concrete, typically ranging from 5000 to 13,000 and n is power constant = 3 [16]. However, it is important to note that this relationship, as defined by MC 2020, is intended for use with aggregates significantly larger than those used in this study. Additionally, the presence of interlayers in the printed concrete can further influence this relationship. Therefore, this study determines the values of n and k by fitting the experimental results to a non-linear regression model (see Figs. 16 and 17).

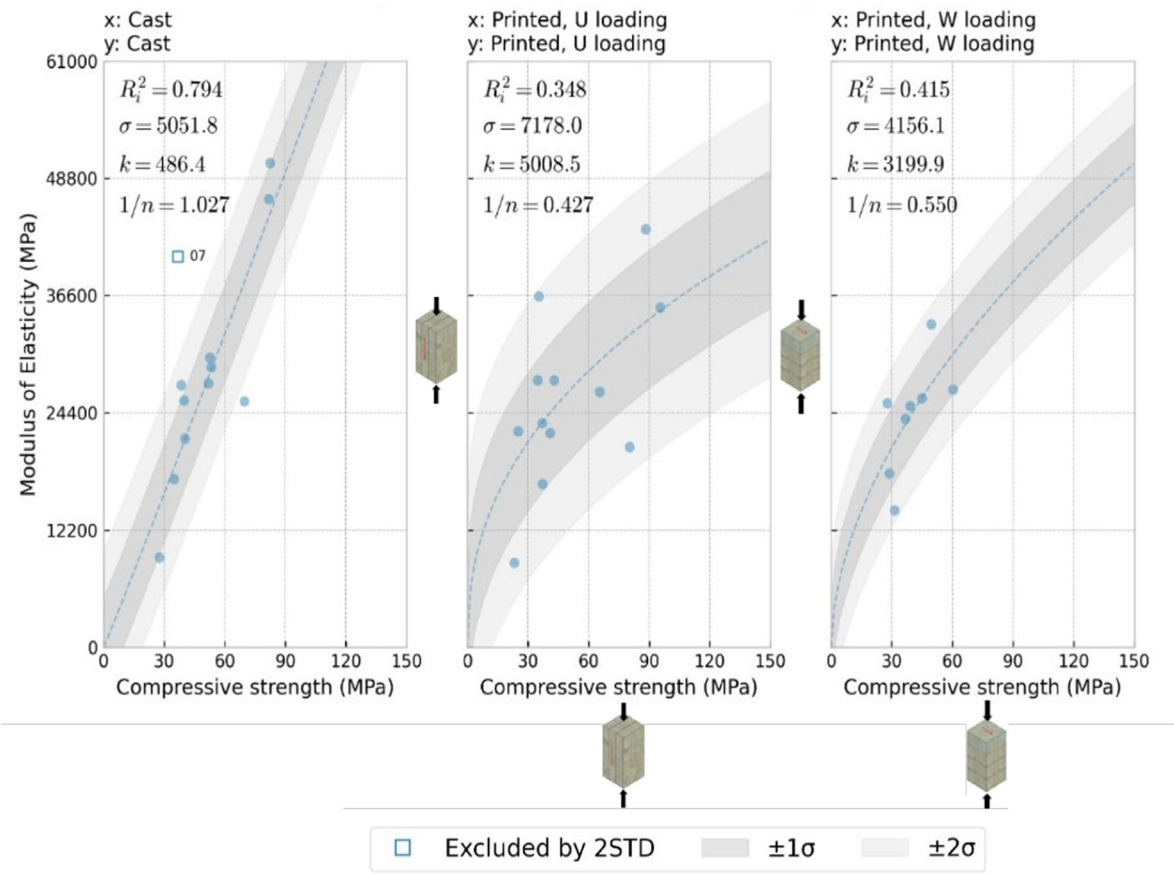


**Fig. 17** Correlating modulus of elasticity (MOE) with compressive strength of mortar-scale specimens prepared in default condition. Images from left to right represent cast specimens and printed specimens tested in U and W loading direction. The MOE and compressive strength were determined using the same specimens

$$\text{MOE} = k.f_c^{\frac{1}{n}} \quad (1)$$

The laboratories determined compressive strength using two types of specimens. The first type included specimens that were used to measure the MOE; these specimens underwent cyclic pre-loading before their compressive strength was measured. The second type consisted of specimens that were not used for MOE measurements, and the compressive strength values from these specimens were discussed in the previous sections. Additionally, prismatic specimens were used for MOE determination, whereas cube specimens were used for the compressive strength measurements in the earlier sections. Notably, the aspect ratios of these specimens were different in both cases. Table 2 compares the compressive strength values determined using the two types of specimens, revealing significant variations for some laboratories. Therefore, the relationship between the MOE and compressive strength was determined for both types of specimens as shown in Figs. 16 and 17. It is worth mentioning that the number of data points used for the correlation differs from what is shown in the table because the table includes only the laboratories that determined compressive strength using both types of specimens for comparison. Some laboratories provided compressive strength data using only one type of specimen and thus could not be included in the comparison. Furthermore, in Figs. 16 and 17, laboratories that tested the compressive strength and MOE with an age difference of more than 3 days were excluded, as in the previous sections.

**Table 2** Average compressive strength and standard deviation determined using specimens which were used to measure the modulus of elasticity and the specimens which were used solely to measure compressive strength

| Lab number | Compressive strength—MOE specimens (MPa) | Standard deviation—MOE specimens (MPa) | Compressive strength (MPa) | Standard deviation (MPa) | Difference in compressive strengths (%) | Difference in standard deviation (%) |
|---|---|---|---|---|---|---|
| *Cast specimens* | | | | | | |
| 01 | 52.7 | 3.8 | 33.1 | 0.9 | − 59.5 | − 327.4 |
| 02 | 34.9 | 2.1 | 35.8 | 1.3 | 2.4 | − 51.8 |
| 04 | 51.9 | 2.0 | 49.8 | 3.7 | − 4.1 | 46.8 |
| 07 | 36.6 | 2.1 | 54.6 | 2.4 | 32.8 | 16.3 |
| 08 | 38.4 | 11.6 | 59.6 | 1.3 | 35.5 | − 755.8 |
| 15 | 39.8 | 4.7 | 42.2 | 5.6 | 5.7 | 15.7 |
| 19 | 82.5 | 9.6 | 120.1 | 3.0 | 31.3 | − 217.8 |
| 23 | 53.4 | 5.6 | 67.6 | 2.5 | 21.0 | − 120.7 |
| 25 | 40.3 | 0.3 | 40.3 | 3.8 | 0.1 | 91.1 |
| *Printed specimens (U loading direction)* | | | | | | |
| 01 | 34.8 | 2.3 | 44.2 | 2.8 | 21.1 | 17.8 |
| 02 | 37.2 | 0.7 | 35.0 | 3.5 | − 6.4 | 77.7 |
| 03 | 80.4 | 16.4 | 38.1 | 6.1 | − 111.0 | − 169.1 |
| 04 | 43.0 | 1.8 | 38.7 | 9.2 | − 10.9 | 79.8 |
| 07 | 35.4 | 2.8 | 63.1 | 2.5 | 43.7 | − 16.2 |
| 08 | 25.2 | 2.4 | 46.8 | 8.8 | 46.1 | 71.5 |
| 15 | 37.1 | 5.8 | 33.5 | 4.1 | − 10.7 | − 42.6 |
| 19 | 95.5 | 19.7 | 88.2 | 3.6 | − 8.2 | − 445.1 |
| 25 | 41.1 | 1.0 | 44.7 | 1.9 | 8.1 | 46.3 |
| 25_b | 23.3 | 4.2 | 20.2 | 1.9 | − 15.1 | − 114.3 |
| 25_c | 65.6 | 2.6 | 50.7 | 7.1 | − 29.3 | 63.1 |
| 28_a | 88.3 | 16.5 | 109.8 | 5.1 | 19.5 | − 227.1 |
| *Printed specimens (W loading direction)* | | | | | | |
| 01 | 27.8 | 3.9 | 39.1 | 3.6 | 28.5 | − 6.7 |
| 02 | 31.4 | 0.5 | 30.2 | 1.9 | − 4.1 | 72.6 |
| 04 | 39.2 | 5.5 | 38.0 | 4.9 | − 3.1 | − 11.6 |
| 07 | 49.6 | 1.6 | 70.8 | 3.7 | 29.9 | 55.0 |
| 08 | 36.8 | 2.2 | 31.6 | 2.2 | − 16.4 | 1.2 |
| 15 | 28.9 | 7.4 | 28.4 | 3.4 | − 1.4 | − 117.9 |

The MOE demonstrated a stronger correlation with compressive strength when specimens were tested separately for MOE and compressive strength (refer to Fig. 16). This improved correlation was observed regardless of differences in aspect ratio between the MOE and compressive strength specimens. Meanwhile, when the MOE was related to the compressive strength determined using the same specimens, the correlation was weaker (see Fig. 17), especially for printed specimens. For cast specimens, the correlation, indicated by $R_i^2$, was higher when the same specimens were used to determine both MOE and compressive strength. However, this relationship became almost linear, possibly due to the lack of data in the high compressive strength range (> 90 MPa). Given the strong correlation and the broader data range, Fig. 16 was selected for further analysis. Compared to cast specimens, the k values increased for printed specimens in the U loading direction but decreased in the W

direction. Meanwhile, the n values also increased for both loading directions, with a more pronounced increase in the U direction. Physically, the k and n values can be interpreted as indicators of the heterogeneity in the concrete mix. To elaborate, in lower strength mixes, where there is a greater difference in properties between the matrix and aggregates (indicating more heterogeneity), the slope (k) tends to be higher. In contrast, in higher compressive strength mixes, where the differences in properties are less pronounced and the material is more homogeneous, the ratio between the MOE and compressive strength (the slope k) decreases. These varying slopes at different compressive strengths ultimately lead to a non-linear relationship between MOE and compressive strength, which is characterized by the value of *n*. Therefore, any observed changes in the n and k values between cast and printed specimens can likely be attributed to the heterogeneity introduced during the 3D printing process. This includes factors like the presence of interlayers as the mix and curing conditions were kept constant for both cast and printed specimens. It was found that the addition of interlayers adversely affected the MOE more than the compressive strength, as shown in Fig. 16. For example, to achieve an MOE of 44,000 MPa, cast specimens required a compressive strength of around 90 MPa, whereas printed specimens needed approximately 120 MPa.

It can be reasonably concluded that the relationship between MOE and compressive strength differs between cast and printed specimens. The current data suggests that 3D printing has a more pronounced negative impact on MOE, particularly in the high compressive strength range, compared to compressive strength itself. As a result, achieving a specific MOE in printed specimens would require a mix with higher compressive strength compared to cast specimens. However, further investigation with more data points is necessary before drawing any definitive conclusions.

## 5 Conclusions

In this RILEM Interlaboratory Study, the compressive strength and modulus of elasticity of printed concrete were analyzed and discussed. The influence of 3D printing process, including the presence of interlayers, on these properties was examined by comparing printed and cast specimens. Additionally, the study assessed the impact of practical issues within printed specimens, such as the presence of cold joints and shifts in curing conditions from standard water bath to ambient curing. The key conclusions and corresponding recommendations from this study are outlined below. These conclusions are based on trends observed by averaging the compressive properties determined by various laboratories. While it is probable that new materials and processing parameters will follow similar trends, this cannot be assured.

1. The extraction location of the specimens from the printed parts did not significantly impact the compressive strength. However, caution is advised in cases where irregularities are more likely at certain locations, such as the bottom section due to dry print beds or top section due to surrounding conditions with low humidity. In these instances, samples taken from the middle section tend to provide a more accurate characterization.
2. The compressive strength of the cast specimens showed a fairly good correlation with that of the printed specimens. Approximately a 25% reduction in compressive strength was observed in the V and W loading directions when the mix was printed instead of casting. The reduction was lowest in the U loading direction, which, however, also exhibited a lower degree of correlation.
3. In most cases, cast specimens yielded higher compressive strength than printed specimens. However, in situations where printable concrete was very stiff, potentially leading to issues with uniform compaction, an opposite trend was observed.
4. The scale of the printed specimens (mortar-scale or concrete-scale) influenced the compressive strength. Larger specimens (concrete-scale) generally exhibited lower compressive strength compared to smaller, mortar-scale specimens, consistent with trends observed in traditional cast concrete. However, when the extraction method was changed to core-drilling, the concrete-scale specimens exhibited higher strength than the mortar-scale specimens, contradicting the previ-

ous trend. Therefore, careful consideration must be given to specimen size and extraction technique when characterizing the strength of printed parts.

5. The compressive strength of printed specimens with cold joints showed a strong correlation with the compressive strength of printed specimens without cold joints. This suggests that the effect of cold joints on compressive strength can be reasonably predicted using available compressive strength data from default conditions. The difference in compressive strength between specimens with and without cold joints was most pronounced in the V loading direction and least significant in the W loading direction.
6. When curing conditions were changed from water bath to ambient curing, no significant change in compressive strength was observed. However, the degree of correlation, indicated by $R^2$, was high for the W and V loading directions (~0.90) but lower for the U loading direction (~0.70). Similar to the effect of cold joints, the compressive strength of printed specimens under ambient curing conditions can be predicted using available data from water bath curing, though caution is advised when interpreting results for the U loading direction.
7. The interlayers introduced during the 3D printing process had a more pronounced effect on the modulus of elasticity of the specimens than on the compressive strength. Although additional data is needed to draw definitive conclusions, the current findings suggest that to achieve the same modulus of elasticity, concrete needs to be designed for a higher compressive strength when printed compared to when it is cast.

Lastly, the TC 304-ADC intends to develop RILEM Recommendations to determine the mechanical properties of 3D-printed concrete based on the Study Plan, the results of this study, and the evaluation of the applied experimental procedures, as presented in this article and the associated papers and data sets [8–10].

**Acknowledgements** The authors express their sincere gratitude to all 30 laboratories that have contributed to this interlaboratory study and the associated persons, in particular: Carolina M. Rangel, Eric Wijen, Naomi van Hierden, Albanela Dulaj (Eindhoven University of Technology), Emre Ortemiz (ISTON), Zeynep Basaran Bundur (Ozyegin University), Jaime Mata-Falcón, Lukas Gebhard, Ana Anton, Che Wei Lin, Ming-Yang Wang (ETH Zurich), Rafael Pileggi (University of São Paulo), Amar Yahia, Masoud Hosseinpoor, Belkis Selma Aouichat, Yacine Hani Bouchilaoun, José Vidal Gonzalez Avina, Shahab Azizi (Université de Sherbrooke), Jiří Vambera (ICE Industrial Services), Tomaž Simon, Rafael Kajzer (Slovenian National Building and Civil Engineering Institute), Passarin Jongvisuttisun (SCG Thailand), Jay Sanjayan (Swinburne University of Technology), Dietmar Stephan (Technical University of Berlin), Steffen Müller (TUD Dresden University of Technology), Denisa Jancarikova (Research Institute for Building Materials, Czech Republic), James Dobrzanski, and Jie Xu (Loughborough University). Furthermore, the following research funding is gratefully acknowledged: National Key R&D Program of China (No. 2023YFC3806902) by author Zhao. Finally, the gracious supply of materials and/or use of facilities is appreciated of: Saint-Gobain Weber Beamix by authors Versteege and Wolfs, Istanbul Concrete Elements and Ready Mixed Concrete Factories (ISTON) by authors Ozturk and Ozyurt, PERI 3D Construction GmbH by authors Richter and Jungwirth, Heidelberg Materials by authors Bos, Auer, Hechtl and Dahlenburg.

**Funding** Open Access funding enabled and organized by Projekt DEAL. For author Zengfeng Zhao, funding was provided by Key Technologies Research and Development Program, Grant NO. 2023YFC3806902.

**Data availability** The study plan for this interlaboratory study on mechanical properties of 3D printed concrete is publicly available on mediaTUM at https://doi.org/10.14459/2023mp1705940. The processed and selected results used for the analyses presented in this paper have been published as dataset on Zenodo at https://doi.org/10.5281/zenodo.12200570. This dataset is only available to participating laboratories until the embargo date 1.7.2025. After that, it will be publicly accessible.

## References


1. Mechtcherine V, Nerella VN, Will F, Näther M, Otto J, Krause M (2019) Large-scale digital concrete construction – CONPrint3D concept for on-site, monolithic 3D-printing. Autom Constr 107:102933. https://doi.org/10.1016/j.autcon.2019.102933
2. Şahin HG, Mardani-Aghabaglou A (2022) Assessment of materials, design parameters and some properties of 3D printing concrete mixtures; a state-of-the-art review. Constr Build Mater 316:125865. https://doi.org/10.1016/j.conbuildmat.2021.125865
3. Muthukrishnan S, Ramakrishnan S, Sanjayan J (2021) Effect of alkali reactions on the rheology of one-part 3D printable geopolymer concrete. Cement Concr Compos 116:103899. https://doi.org/10.1016/j.cemconcomp.2020.103899
4. Le TT, Austin SA, Lim S, Buswell RA, Law R, Gibb AGF, Thorpe T (2012) Hardened properties of high-performance printing concrete. Cem Concr Res 42(3):558–566. https://doi.org/10.1016/j.cemconres.2011.12.003
5. Wolfs R, Bos F, Salet T (2019) Hardened properties of 3D printed concrete: The influence of process parameters on interlayer adhesion. Cem Concr Res 119:132–140. https://doi.org/10.1016/j.cemconres.2019.02.017
6. Bos F, Mechtcherine V, Roussel N, Menna C, Wolfs R, Lombois-Burger H, Baz B, Weger D, Moro S, Nematollahi B, Santhanam M, Zhang Y, Bhattacherjee S, Jia Z, Chen Y (2023) RILEM TC 304-ADC ILS-mech Study Plan, 13.04.2023. Published on MediaTUM. https://doi.org/10.14459/2023mp1705940
7. Muthukrishnan S, Ramakrishnan S, Sanjayan J (2021) Technologies for improving buildability in 3D concrete printing. Cement Concr Compos 122:104144. https://doi.org/10.1016/j.cemconcomp.2021.104144
8. Wolfs R, Versteege J, Santhanam M, Bhattacherjee S, Bos F, Robens-Radermacher A, Muthukrishnan S, Menna C, Ozturk O, Ozyurt N, Roupec J, Richter C, Jungwirth J, Miranda L, Ammann R, Caron JF, de Bono V, Monte R, Navarrete I, Eugenin C, Lombois-Burger H, Baz B, Sinka M, Sapata A, HarbouzI, Zhang Y, Jia Z, Kruger J, Mostert JP, Šter K, Šajna A, Kaci A, Rahal S, Snguanyat C, Arunothayan A, Zhao Z, Mai I, Rasehorn IJ, Böhler D, Freund N, Lowke D, Neef T, Taubert M, Auer D, Hechtl CM, Dahlenburg M, Esposito L, Buswell R, Kolawole J, Isa MN, Liu X, Wang Z, Subramaniam K, Mechtcherine V (2025) Mechanical Properties of 3D Printed Concrete: a RILEM TC 304-ADC Interlaboratory Study—Flexural and Tensile Strength. Manuscript accepted for this Materials & Structures Topical Issue. https://doi.org/10.1617/11527-025-02687-w
9. Bos F, Menna C, Robens-Radermacher A, Wolfs R, Roussel N, Lombois-Burger H, Baz B, Weger D, Nematollahi B, Santhanam M, Zhang Y, Bhattacherjee S, Jia Z, Chen Y, Mechtcherine V (2025) Mechanical properties of 3D printed concrete: a RILEM TC 304-ADC Interlaboratory Study—approach and main results. Manuscript accepted for this Materials & Structures Topical Issue. https://doi.org/10.1617/s11527-025-02686-x
10. Bos F, Robens-Radermacher A, Mechtcherine V (2025) Database of the RILEM TC 304-ADC interlaboratory study on mechanical properties of 3D printed concrete (ILS-mech). 2024. https://doi.org/10.5281/zenodo.12200570. Embargoed until 1 July 2025
11. Robens-Radermacher A, Kujath C, Bos F, Mechtcherine V, Unger JF (2025) Mechanical Properties of 3D Printed Concrete: a RILEM TC 304-ADC Interlaboratory Study—Design and Implementation of a Database System for Querying, Sharing and Analyzing Experimental Data. Manuscript accepted for this Materials & Structures Topical Issue. https://doi.org/10.1617/s11527-025-02650-9
12. EN 12390–13: (2021): Testing hardened concrete - Part 13: Determination of secant modulus of elasticity in compression
13. EN 196–1: (2016) : Methods of Testing Cement – Part 1: Determination of Strength
14. ASTM C1437–07: Standard Test Method for Flow of Hydraulic Cement Mortar. https://doi.org/10.1520/C1437-07
15. Neville A (2012) Properties of Concrete 5th edition (Harlow. 2012, Pearson Education. https://www.academia.edu/download/52236036/properties-of-concrete-by-am-neville.pdf
16. Tošić N, Torrenti JM, Sedran T, Ignjatović I (2021) Toward a codified design of recycled aggregate concrete structures: Background for the new fib Model Code 2020 and Eurocode 2. Struct Concr 22(5):2916–2938. https://doi.org/10.1002/suco.202000512